AD-A112 264 FORD AEROSPACE AND COMMUNICATIONS CORP NEWPORT BEACH --ETC F/G 7/4
CONTINUUM ABSORPTION BY H2O.(U)
MAR 82 D E BURCH F19628-79-C-0041
UNCLASSIFIED U-6696 AFGL-TR-81-0300 NL

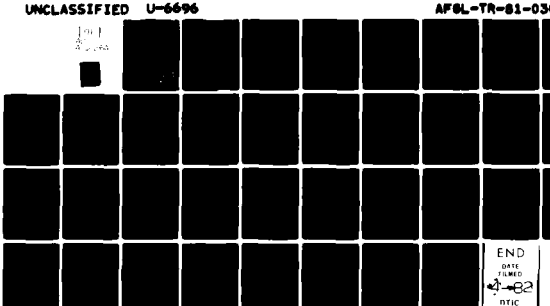

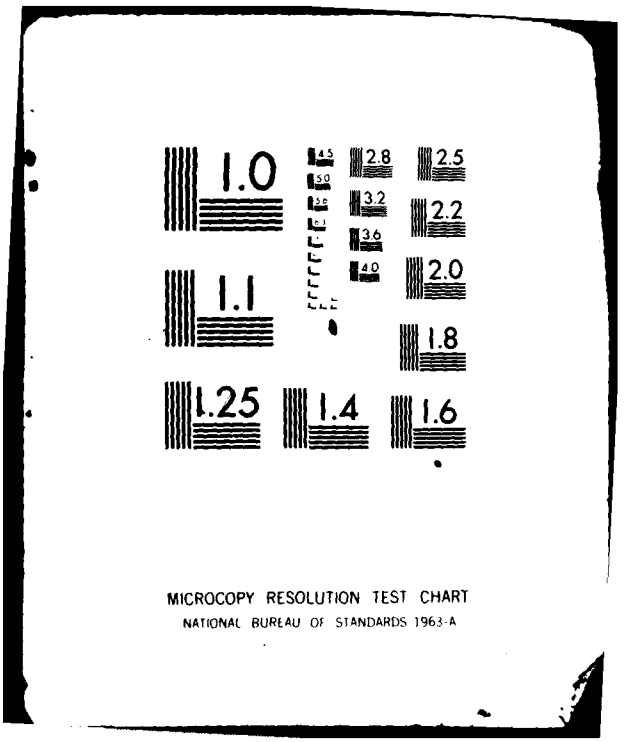
1.0
1.1
1.25
1.4
1.6
1.8
2.0
2.2
2.5
2.8
3.2
3.6
4.0
4.5
5.0
5.6
MICROCOPY RESOLUTION TEST CHART
NATIONAL BUREAU OF STANDARDS 1963-A

(12)

AFGL-TR-81-0300

CONTINUUM ABSORPTION BY H_2O

Darrell E. Burch

Ford Aerospace and Communications Corporation
Aeronutronic Division
Ford Road, Newport Beach, CA 92663

March 1982

Final Report for Period January 1979 - November 1981

Approved for public release; distribution unlimited

AIR FORCE GEOPHYSICS LABORATORY
AIR FORCE SYSTEMS COMMAND
UNITED STATES AIR FORCE
HANSCOM AFB, MASSACHUSETTS 01731

Unclassified

SECURITY CLASSIFICATION OF THIS PAGE (When Data Entered)

REPORT DOCUMENTATION PAGE		READ INSTRUCTIONS BEFORE COMPLETING FORM
1. REPORT NUMBER AFGL-TR-81-0300	2. GOVT ACCESSION NO. AD-A112264	3. RECIPIENT'S CATALOG NUMBER
4. TITLE (and Subtitle) Continuum Absorption by H_2O		5. TYPE OF REPORT & PERIOD COVERED Final Report Jan 1979 - Nov 1981
		6. PERFORMING ORG. REPORT NUMBER U-6696 ✓
7. AUTHOR(s) Darrell E. Burch		8. CONTRACT OR GRANT NUMBER(s) F19628-79-C-0041
9. PERFORMING ORGANIZATION NAME AND ADDRESS Ford Aerospace and Communications Corporation Aeronutronic Division Ford Road, Newport Beach, CA. 92663		10. PROGRAM ELEMENT, PROJECT, TASK AREA & WORK UNIT NUMBERS 62101F 767009AI.
11. CONTROLLING OFFICE NAME AND ADDRESS Air Force Geophysics Laboratories Hanscom AFB, Massachusetts 01731 Contract Monitor: Anthony P. D'Agati OPI		12. REPORT DATE March 1982
		13. NUMBER OF PAGES 46
14. MONITORING AGENCY NAME & ADDRESS(if different from Controlling Office)		15. SECURITY CLASS. (of this report) Unclassified
		15a. DECLASSIFICATION DOWNGRADING SCHEDULE

16. DISTRIBUTION STATEMENT (of this Report)

Approved for public release; distribution unlimited

17. DISTRIBUTION STATEMENT (of the abstract entered in Block 20, if different from Report)

18. SUPPLEMENTARY NOTES

19. KEY WORDS (Continue on reverse side if necessary and identify by block number)

H_2O
Atmospheric Transmission
Absorption
Continuum Absorption
ine Shape

20. ABSTRACT (Continue on reverse side if necessary and identify by block number)

Data on the H_2O continuum absorption obtained by many different workers from laboratory samples and atmospheric paths are compared in the various windows in the infrared, millimeter-wave and microwave regions. Values of the continuum absorption coefficients calculated on the basis of simple, widely used line shapes may differ greatly from observed values in the

DD FORM 1 JAN 73 1473 EDITION OF 1 NOV 65 IS OBSOLETE

Unclassified

SECURITY CLASSIFICATION OF THIS PAGE (When Data Entered)

windows between strong absorption lines. The temperature dependence of this absorption is also not predictable from present day understanding of line shapes or of dimers, which are thought by many to contribute. The shapes of self-broadened H_2O lines are quite different from those of N_2-broadened lines, and the difference increases with increasing distance from the centers of the lines. Several characteristics of the continuum absorption are common throughout the windows from the infrared to the microwave region.

CONTENTS

LIST OF FIGURES

SECTION 1
INTRODUCTION AND SUMMARY

Water vapor is responsible for much of the lower-atmosphere absorption in the infrared, millimeter-wave, and microwave windows. Wide variations in the atmospheric temperature and humidity lead to wide variations in the attenuation in these windows. Although the positions, intensities and widths of most of the significant H_2O absorption lines are known, the absorption in the windows cannot be calculated accurately from theoretical considerations alone. Many instruments and complicated systems such as thermal imaging devices, remote sensing systems, seekers, trackers, and laser communications systems are designed to operate in one or more of the atmospheric windows. Thus, a good understanding of the nature of the continuum absorption and the ability to predict it are essential.

The inability to make accurate calculations is due to the lack of knowledge about the shapes of the absorption lines and about possible absorption by dimers consisting of two bound H_2O molecules or by clusters of several molecules. The amount of H_2O absorption by a given atmospheric path is much greater in some windows than in others. In essentially all of the spectral windows, the absorption measured in the laboratory or in the atmosphere is greater than that predicted on the basis of the known[1] positions, intensities and widths of the lines, and previously adopted theoretical line shapes. Several very weak H_2O absorption lines occur in any of the infrared windows, but most of the lower-atmosphere absorption within the windows is due to the continuum absorption. Many experimenters have attempted to measure the continuum absorption under a wide variety of conditions and by different methods. The data have also been analyzed in a variety of ways, and quite diverse conclusions have been drawn.

Section 2 summarizes H_2O continuum measurements made under widely different conditions by several experimenters from the infrared to the microwaves. The data in the different spectral regions have been analyzed in a manner similar to the one used previously by us in the infrared. Several characteristics of the continuum are common throughout the spectrum, and the results suggest strongly that most of the continuum is due to the extreme wings of absorption lines. No solid evidence of spectral structure due to H_2O dimers or clusters has been observed.

---

[1] R. A. McClatchey, W. S. Benedict, S. A. Clough, D. E. Burch, R. F. Calfee, K. Fox, L. S. Rothman, and J. S. Garing, AFCRL-TR-73-0096, U. S. Air Force (1973). (Available from NTIS.)

SECTION 2
COMPARISON OF H_2O CONTINUUM ABSORPTION IN DIFFERENT SPECTRAL REGIONS

This section compares the results of measurements of the H_2O continuum in the well-known 4 μm and 8-13 μm windows and at many wavenumbers of minimum absorption in very narrow windows only a few cm^{-1} from strong infrared absorption lines. Results of similar measurements are also shown for the millimeter-wave and microwave regions. Historically, the results obtained in the millimeter-wave and microwave regions have been analyzed by methods different from those used in the infrared. Results presented herein show that the absorption data have several common characteristics in all of the spectral regions if the methods of analysis are similar. It is important that the effects of self broadening and N_2 broadening (to simulate air broadening) be treated separately.

The most serious discrepancies between calculated and measured H_2O absorption occur in spectral regions far enough from the significant absorption lines that very little of the absorption can be attributed to lines centered within several cm^{-1}. Measurements in these regions almost always show "excess" absorption, i.e., the experimental values are greater than values calculated by employing theoretical line shapes that have been used widely in the infrared and millimeter-wave regions. The excess absorption is too great to be due to possible errors in the intensities, widths, and positions of the absorption lines listed in Reference 1.

The excess absorption has four common characteristics in the windows from the infrared to the microwaves:

1. It has the nature of continuum; that is, it does not change rapidly with changing wavenumber.

2. It decreases rapidly with increasing temperature.

3. It is much greater for self broadening (pure H_2O vapor) than for N_2 broadening of the H_2O lines (mixtures of $H_2O + N_2$).

4. The percentage discrepancy between experiment and theory is greater in regions of weak absorption than in regions of medium or strong absorption.

Much of the material in this section was presented at a recent meeting of SPIE, the Society of Photo-Optical Instrumentation Engineers, and is available in the proceedings:

[2]D. E. Burch, SPIE Proceedings 277, (1981).

Among the several suggested sources of this poorly understood absorption are: (a) extreme wings of absorption lines of the H_2O molecules (monomers), (b) dimers (H_2O:H_2O) consisting of two H_2O molecules bound together in an equilibrium state,[2] [3-6] (c) dimers in a nonequilibrium state,[7] (d) ionic clusters consisting of several H_2O molecules,[8] and (e) uncharged clusters of H_2O molecules.[9,10] Many workers believe that the first source, the extreme wings of lines, is not responsible for a significant amount of the absorption in the principal atmospheric windows. This conclusion is based largely on the failure of current theories on line broadening to predict the amount of absorption observed in these windows at any temperature or the strong negative temperature dependence that is observed. Dimers and clusters of H_2O molecules are known to exist and to decrease rapidly in population with increasing temperature. Thus, it is natural that these polymolecular species have been considered as possible sources of the excess absorption. However, there are no spectral features of this extra absorption in water vapor in equilibrium that can be attributed without question to a particular vibrational or rotational mode of a dimer or cluster of H_2O molecules. The number of dimers or clusters expected in samples in thermal equilibrium also falls far short of the number required to produce the amount of excess absorption that is observed.

Clough, et al,[11-12] have recently compared observed H_2O continuum data with calculations based on an extension of a line shape derived by Van Vleck

---

[3] K. Bignell, Quart. J. Roy. Meteorol. Soc. 96, 390 (1970).

[4] S. S. Penner, J. Quant. Spectrosc. Radiat. Transfer 13, 383 (1973).

[5] W. J. Burroughs, R. G. Jones, and H. A. Gebbie, J. Quant. Spectrosc. Radiat. Transfer 9, 809 (1969).

[6] M. T. Coffey, Quart. J. Roy. Meteorol. Soc. 103, 685 (1977).

[7] D. T. Llewellyn-Jones, R. J. Knight, and H. A. Gebbie, Nature 274, 876 (1978).

[8] H. R. Carlon, Infrared Physics 19, 49 (1979).

[9] H. R. Carlon, Tech. Report ANCSL-TR-79013, U. S. Army Armament Research and Development Command (1979). (Available from NTIS.)

[10] H. R. Carlon, Infrared Physics 19, 549 (1979).

[11] S. A. Clough, F. X. Kneizys, R. Davies, R. Camache, and R. Tipping, Theoretical Line Shape for H_2O Vapor: Application to Continuum in Atmospheric Water Vapor (A. Deepak, T. D. Wilkerson, and L. H. Ruhnke, eds.), Academic Press, New York (1980).

[12] S. A. Clough, F. X. Kneizys, L. S. Rothman, and W. O. Gallery, SPIE Proceedings 277 (1981).

and Huber[13] (VVH). These comparisons indicate that, contrary to previous work, there is a shortage, not an excess, of absorption in some of the windows. This quite different conclusion is reached because the recent VVH line shape predicts much more absorption in the extreme wings of the lines than do the previously used shapes. A thorough discussion of the theoretical basis for the various line shapes is beyond the scope of this paper. However, it is important to note that no theoretical line shape, without some empirical modification, predicts accurately the absorption in the extreme wings of absorption lines of H_2O, or of other gases besides H_2O.

The main objective of the various investigations summarized here has been to provide a means of including an empirical continuum absorption in line-by-line calculations so that the absorption can be computed correctly. The theoretical line shapes used in these studies were the traditional ones (see Table 1 below) that predict less absorption than is observed. Thus, the empirical continuum represents an excess absorption. Because of the different characteristics of the various windows, somewhat different approaches have been used.

LINE SHAPES AND PARAMETERS

Table 1 summarizes five theoretical line shapes that have been used for collision-broadened lines. Each of these theoretical shapes is derived from a different set of assumptions about the nature and influence of collisions, but all five of the shapes become equivalent near the line center where $| \nu - \nu_o | << \nu$. Any one of these shapes agrees very well with experimental measurements made in the infrared within a few cm^{-1} of the centers of the absorbing lines, but none adequately describes the extreme wing absorption. Experimental data can frequently be explained in terms of an empirical line formed as a product of one of the theoretical shapes and a correction factor χ as discussed in Table 1.

It has been well established experimentally that the intensities of most absorption lines are essentially independent of α. For a line shape to be exact, the line intensity S must be related to the absorption coefficient k given by the shape equation by:

$$S = \int_0^\infty k \, d\nu \qquad (1)$$

It can be shown that this equation is not valid for all of the theoretical line shapes listed in Table 1. This has not been considered a serious problem for most practical purposes in the past because it was assumed that the shape would become invalid in the extreme wings where $| \nu - \nu_o |$ is very large.

---

[13] J. H. Van Vleck and D. L. Huber, Rev. Mod. Phys. 49, 939 (1977).

TABLE 1. THEORETICAL AND EMPIRICAL LINE SHAPES

$\frac{S}{\pi} \frac{\alpha}{(\nu-\nu_o)^2 + \alpha^2}$	Simple Lorentz
$\frac{S}{\pi} \frac{4\nu^2\alpha}{(\nu^2-\nu_o^2)^2 + 4\nu^2\alpha^2}$	Gross
$\frac{S}{\pi} \left[\frac{\nu}{\nu_o} \frac{\nu}{2\kappa\theta}\right] \left[\frac{\alpha}{(\nu-\nu_o)^2 + \alpha^2} + \frac{\alpha}{(\nu+\nu_o)^2 + \alpha^2}\right]$	VVW
$\frac{S}{\pi} \frac{\nu}{\nu_o} \frac{1 - \exp(-ch\ \nu/\kappa\theta)}{1 - \exp(-ch\ \nu_o/\kappa\theta)} \left[\frac{\alpha}{(\nu-\nu_o)^2 + \alpha^2} + \frac{\alpha}{(\nu+\nu_o)^2 + \alpha^2}\right]$	MVVW
$\frac{S}{\pi} \frac{\nu}{\nu_o} \frac{\tanh(hc\nu/2\kappa\theta)}{\tanh(hc\nu_o/2\kappa\theta)} \left[\frac{\alpha}{(\nu-\nu_o)^2 + \alpha^2} + \frac{\alpha}{(\nu+\nu_o)^2 + \alpha^2}\right]$	VVH

VVW, MVVW and VVH are abbreviations for Van Vleck-Weisskopf, modified Van Vleck-Weisskopf, and Van Vleck-Huber, respectively. ν_o, line center; α, halfwidth; S, line intensity as defined in reference 1; κ, Boltzmann's constant; h, Planck's constant; and θ, temperature in Kelvins.

At a given wavenumber, the absorption coefficient due to a single line may be expressed in terms of the coefficient given by one of the theoretical shapes times an empirical correction factor χ, which is a function of $(\nu-\nu_o)$. As an example:

$$k \text{ (empirical Lorentz)} = \chi\ k \text{ (simple Lorentz)}$$

If $\chi > 1$, for the empirical Lorentz shape, the line is said to be "super Lorentzian"; if $\chi < 1$, the line is said to be "sub-Lorentzian." The corresponding terms apply for the other shapes.

The absorption coefficient for a single line is related to the true transmittance T' of the line that would be observed with infinite resolving power by:

$$k = (-1/u) \ln T' \tag{2}$$

The absorber thickness u is given by:

$$u \text{ (molecules cm}^{-2}) = p(\text{atm})\ 2.69 \times 10^{19} \frac{\text{molecules}}{\text{cm}^3\ \text{atm}} \times \frac{273}{\theta} L \text{ (cm)} \tag{3}$$

where θ is in Kelvins. It follows that the units for S are molecules^{-1} cm^2 cm^{-1}.

The absorption coefficients given by any of the theoretical shapes in Table 1 is proportional to α in the extreme wings where $|\nu - \nu_0| \ll \alpha$. This proportionality relationship appears experimentally to be valid, even when the coefficient is greatly different from that given by any of the theoretical expressions. The halfwidth of a collison-broadened line for a mixture of H_2O in N_2 at a fixed temperature is given by:

$$\alpha = \alpha_S^o\, p + \alpha_N^o\, p_N \tag{4}$$

The partial pressures in atmospheres of the H_2O and N_2 are represented by p_O and p_N, respectively. N_2 is frequently used to simulate dry air. Both α_S^o and α_N are assumed to be proportional to $\theta^{-0.62}$, as recommended by Reference 1 for H_2O lines. The equivalent pressure P_e is proportional to α regardless of the relative values of p and p_N.

$$P_e = Bp + p_N = (B - 1)\ p + P \tag{5}$$

where P is the total pressure, and

$$B = \alpha_S^o/\alpha_N^o \quad . \tag{6}$$

B has been determined experimentally to be approximately 5 for H_2O.

The continuum was studied by investigating the absorption at selected wavenumbers where there is little absorption by lines centered within approximately 1 cm^{-1}. However, there may be a small amount of absorption because of these nearby ($|\nu - \nu_0| < |$cm^{-1}) lines, and their contribution to the total absorption coefficient is denoted as k (local). This quantity may vary rapidly with changing wavenumber. For the relatively low sample pressures employed, α for any of the lines is much less than 1 cm^{-1}. Therefore, the contributions by any line for which $|\nu - \nu_0| > 1$ cm^{-1} is proportional to α.

The total absorption coefficient K at a given wavenumber for an H_2O + N_2 mixture is given by the following equation, which also defines the continuum coefficients for self broadening and N_2 broadening:

$$K = (-1/u) \ln T' = K \text{ (Local)} + C_S^o p + C_N^o p_N = K \text{ (local)} + C_S + C_N \quad (7)$$

The attenuation in decibels over a pathlength L due to the continuum is

$$A \text{ (dB)} = A_L \text{ (dB/km) } L\text{(km)} = 3.19 \times 10^{22} L(p^2 C_S^o + p\, p_N\, C_N^o)/\theta \quad (8)$$

All of the continuum data from the laboratory discussed in this report exhibit the pressure dependence indicated by Equations (7) and (8).

800 cm^{-1} TO 1250 cm^{-1} WINDOW

The H_2O absorption in the typical lower atmosphere is dominated by continuum absorption in this well-known window although it also contains many very weak absorption lines. Figure 1 summarizes the results[14] of continuum measurements for pure H_2O at three different temperatures; the very strong negative temperature dependence is apparent. All of the H_2O lines centered between 800 cm^{-1} and 1250 cm^{-1} are very weak and therefore have a very small influence on the continuum curve. An accurate calculation of the absorption spectrum must include the local line absorption as well as the continuum absorption represented by the curve in Figure 1. Although the local lines are very weak, one of them may be the major source of absorption at a wavelength near its center. The continuum curves are based on measurements made between lines where the contribution K (local) by the local lines is very small and can be accounted for adequately.

We[14, 15] have also attempted to measure the N_2-broadening coefficient C_N^o between 800 cm^{-1} and 1200 cm^{-1} for 296K samples, but have found this quantity too small to measure accurately. The results indicate that the ratio of C_S^o/C_N^o in this spectral region is very large, possibly greater than 1000:1. McCoy, et al,[16] have determined this ratio to be approximately 200:1, but a survey by Roberts, et al,[17] of long-path atmospheric measurements indicates that the value of 1000:1 is more nearly correct than 200:1. The large ratio C_S^o/C_N^o leads to the result that the self broadening term in Equation (7) dominates over the N_2 broadening term in the atmosphere if the partial pressure of H_2O is more than approximately 0.01 atm. Therefore, the absorption is approximately proportional to p^2L (see Equation (8)) and becomes very large in tropical atmospheres of high humidity in which p may be as large as 0.04 atm.

---

[14] D. A. Gryvnak, D. E. Burch, R. L. Alt, and D. K. Zgonc, AFGL-TR-76-0246, Final Report, Contract F19628-76-C-0067 (1976). (Available from NTIS.)

[15] D. E. Burch, Semi-Annual Tech. Report, AFCRL Contract No. F19628-69-C-0263, U. S. Air Force (1970). (Available from NTIS.)

[16] J. H. McCoy, D. B. Rensch, and R. K. Long, Appl. Opt. 8, 1471 (1969).

[17] R. E. Roberts, J. E. A. Selby, and L. M. Biberman, Appl. Opt. 15, 2085 (1976).

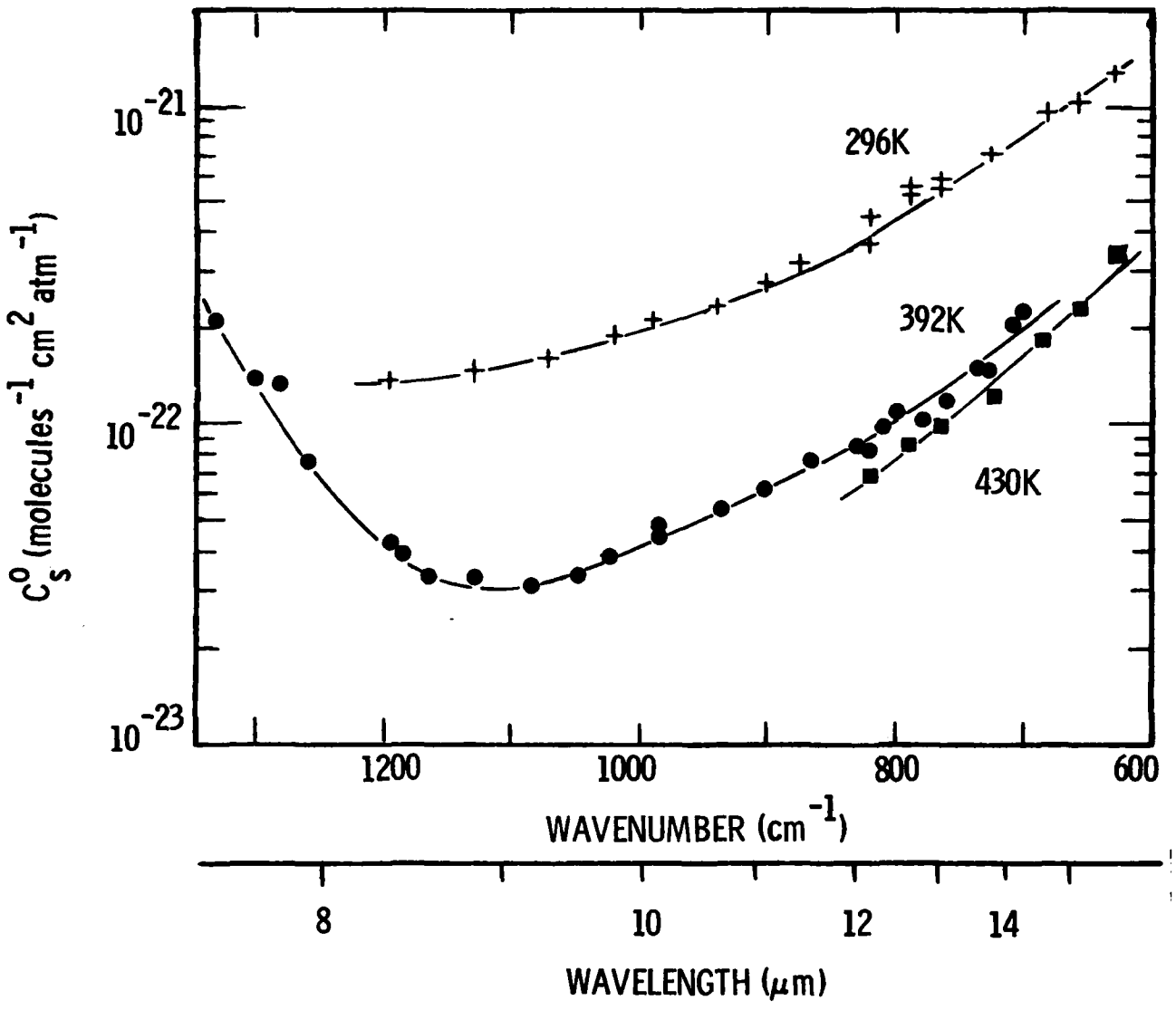

Figure 1. Spectral plots of C_s^o for H_2O at three different temperatures.

2400 cm^{-1} TO 2800 cm^{-1} WINDOW

This window contains several very weak lines of H_2O and HDO, but like the 800 cm^{-1} to 1250 cm^{-1} window, the continuum produces most of the H_2O absorption in the typical lower atmosphere. The three lower curves of Figure 2 summarize results of continuum measurements that we[18] reported in 1971 for pure H_2O at three different elevated temperatures. Because the continuum absorption is very weak, it is difficult to make laboratory samples that produce enough absorption to be measured accurately. Operating at elevated temperatures makes it possible to use high partial pressures of H_2O, which leads to more absorption. The upper curve is based on extrapolation of the other data to 296K.

Since the 1971 data were reported, we and workers in other laboratories have measured the continuum for samples near 296K. Because of the very small absorption and problems due to sample impurities, there is considerable disagreement among the results. The results of the more recent measurements are the subject of a separate report now in preparation. It is apparent that the self-broadening coefficients have a very strong negative temperature dependence and that the N_2-broadening coefficients are much smaller than the corresponding values for self broadening.

333 cm^{-1} TO 825 cm^{-1}

This spectral interval contains many rotational H_2O lines; it overlaps the well-known 800-1250 cm^{-1} window on one end and is bounded on the other end by very strong absorption lines that make the lower atmosphere essentially opaque and over relatively short paths. The extreme wings of these strong lines centered between approximately 40 cm^{-1} and 333 cm^{-1} contribute significantly to the continuum absorption between 333 cm^{-1} and 825 cm^{-1}.

Typical wavenumbers where the continuum was studied[19] are indicated by arrows in Figure 3. The first objective of the measurements was to determine the absorption exclusive of the contribution by local lines centered within approximately 1 cm^{-1} of the wavenumber of observation. The local lines were accounted for as discussed previously.

The transmittance of the continuum was determined at each of the selected wavenumbers for a variety of samples of pure H_2O or $H_2O + N_2$ at different pressures, temperatures and pathlengths. At a given temperature,

---

[18] D. E. Burch, D. A. Gryvnak, and J. D. Pembrook, AFCRL-71-0124, Contract No. F19628-69-0263, U. S. Air Force (1971). (Available from NTIS.)

[19] D. E. Burch and D. A. Gryvnak, AFGL-TR-0054, Final Report, Contract F19628-76-C-0301 (1979).

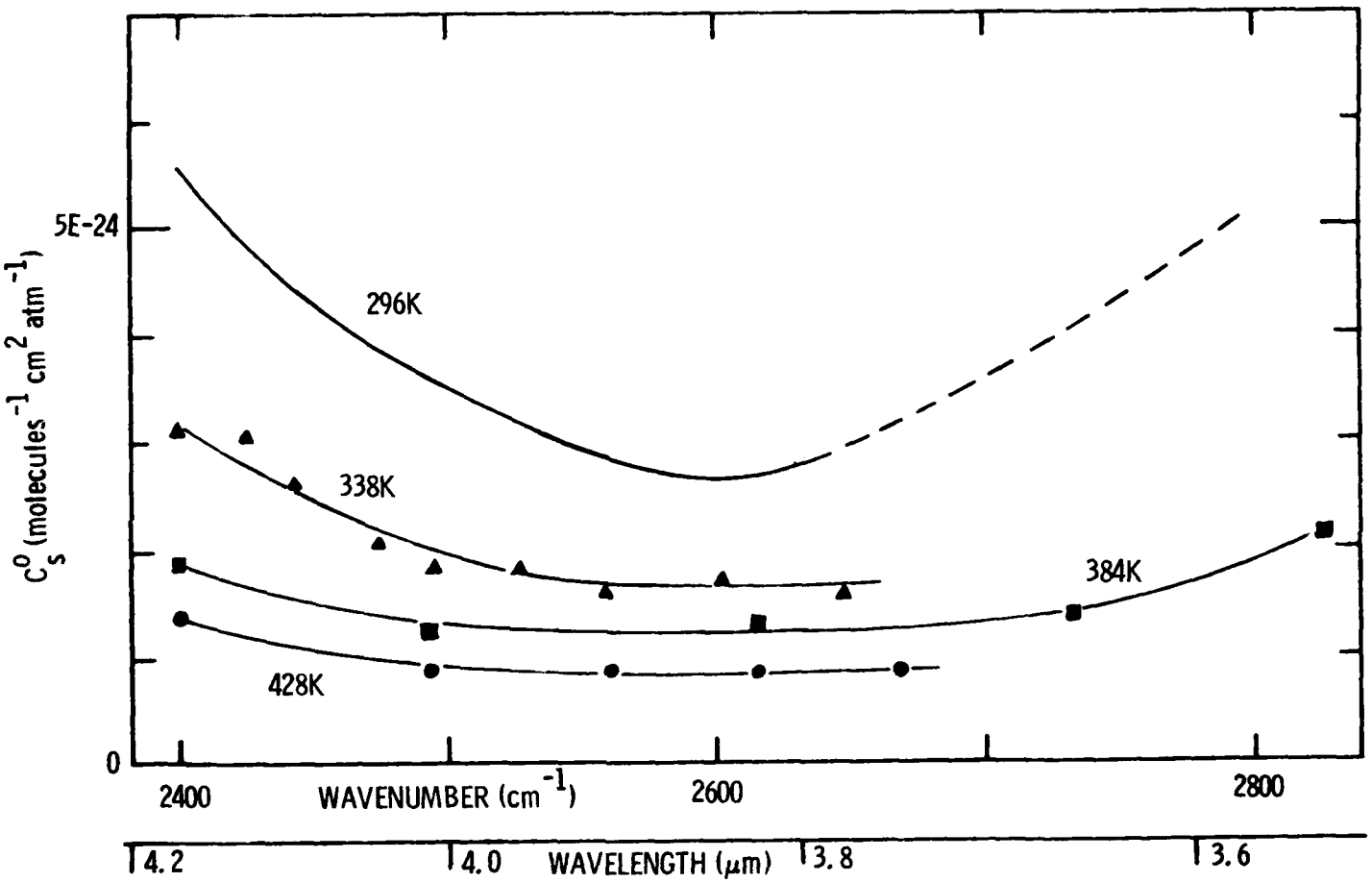

Figure 2. Spectral plots of C_s^o for H_2O at four temperatures. The curve corresponding to 296 K is based on extrapolation from the other three curves. The figure is from a previous report [18]. (18. D. E. Burch, D. A. Gryvnak, and J. D. Pembrook, AFCRL-71-0124, Contract No. F19628-69-0263, U. S. Air Force (1971). (Available from NTIS.)

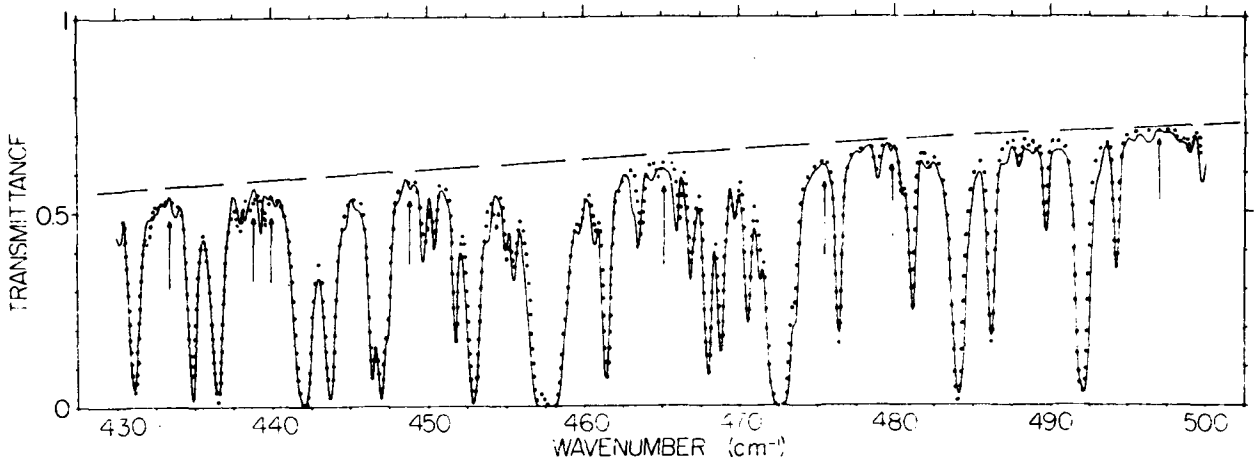

Figure 3. Spectral curve of transmittance for a sample of pure H_2O at 296 K. The vertical arrows designate wavenumbers at which the continuum has been measured. The solid curve represents experimental data. The dots represent values calculated by including the empirical continuum represented by the smooth, broken line. Spectral slitwidth $\simeq 0.3$ cm^{-1}. p = 0.0099 atm, L = 477 m, u = 1.17×10^{22} molecules/cm^2.

the data followed, within expected experimental error, the relationship of Equation (7) and thus made it possible to determine values of C_S^0 and C_N^0. Bignell[3] has measured quantities that correspond directly to C_S^0 and C_N^0 at six different wavenumbers between 497 cm^{-1} and 832 cm^{-1}; his values agree well with those reported here.

Figure 4 shows the results of the determination of the empirical continuum for self broadening at 296 K. The solid squares represent the experimental values of C_S^0. Values represented by the triangles have been calculated by the following procedure:

1. The AFGL[1] line parameters are used as input to a computer program to calculate contributions due to these lines at the selected wavenumbers of maximum transmittance where C_S^0 and C_N^0 have been measured. Only those lines for which $1 < |\nu - \nu_o| \leq 30$ cm^{-1} are included in the calculation. (Recall that the experimental values with which these values are to be compared do not include contributions by lines for which $|\nu - \nu_o| < 1$ cm^{-1}.)

   In summing the contributions due to the lines, the simple Lorentz shape is used for $|\nu - \nu_o| \leq 20$ cm^{-1}. For $20 < |\nu - \nu_o| \leq 30$ cm^{-1}, the contribution included for each line is given by $k = k$ (simple Lorentz) I, where k (simple Lorentz) corresponds to the Lorentz shape and I varies linearly from unity at $|\nu - \nu_o| = 20$ cm^{-1} to zero at $|\nu - \nu_o| = 30$ cm^{-1}. This relation is referred to as an "apodized bound" of 30 cm^{-1}. The term bound is normally used to denote the value of $|\nu - \nu_o|$ beyond which the contribution by a line is not included.

   The value of 30 cm^{-1} for the apodized bound has been selected as a compromise between smoothness of the resulting empirical continuum curve and the computer time required to calculate spectra. If a normal unapodized 30 cm^{-1} bound is used, small discontinuities in the spectra occur at points 30 cm^{-1} from strong lines.

2. The values calculated in step 1 are subtracted from the larger experimental values, represented by solid squares, for the corresponding wavenumbers.

3. The differences calculated in step 2 are plotted as + signs, and a smooth curve is drawn through them. It is significant

---

[1] R. A. McClatchey, W. S. Benedict, S. A. Clough, D. E. Burch, R. F. Calfee, K. Fox, L. S. Rothman, and J. S. Garing, AFCRL-TR-73-0096, U. S. Air Force (1973). (Available from NTIS.)

[3] K. Bignell, Quart. J. Roy. Meteorol. Soc. 96, 390 (1970).

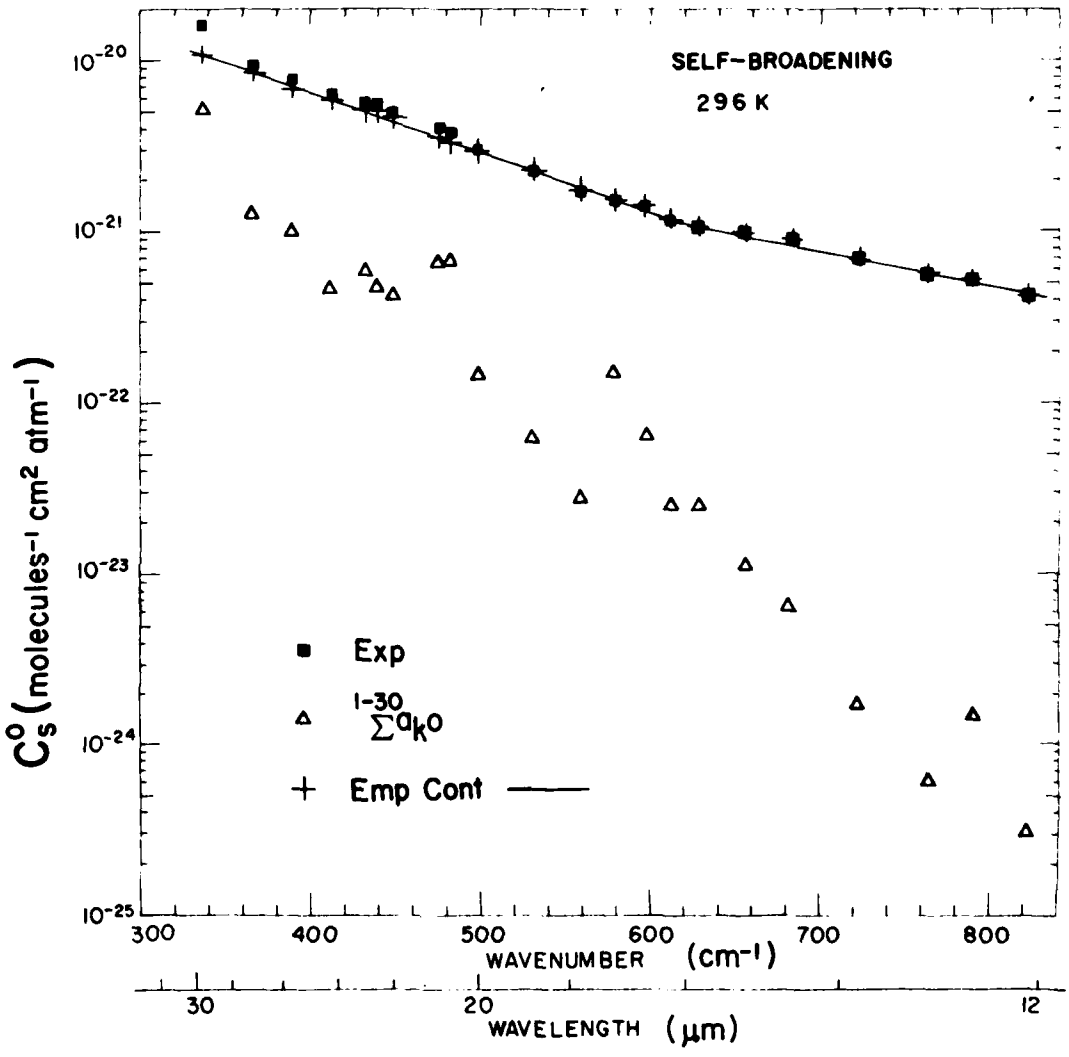

Figure 4: Semi-logarithmic plot of the H_2O continuum coefficient for self broadening at 296 K. The solid squares represent experimental values. The triangles represent values calculated by summing the contributions of lines according to an apodized weighting function. The curve drawn through the +'s represents the empirical continuum.

that nearly all the + signs, which represent the excess absorption required to bring about agreement between calculated and experimental values, fall within approximately 10 percent of the corresponding smooth curve. Thus, it is appropriate to call this an empirical continuum. Slightly better fits to the data might be obtained if some structure with separations between approximately 5 cm^{-1} and 50 cm^{-1} were added to the empirical continuum.

Figures similar to Figure 4 have been drawn,[19] but not included here, to represent self broadening at two elevated temperatures, 338 K and 430 K. As the temperature increases, there is a general decrease in the values for the empirical continuum relative to the corresponding calculated values. Similar figures have also been drawn to represent N_2 broadening at these two temperatures and at room temperature, 296 K. A typical value for the empirical continuum relative to the calculated value at the same wavenumber is seen from Figures 4 and 5 to be less for N_2 broadening than for self broadening. The smaller relative values for the empirical continuum lead to larger percentage errors in their determination. This, in turn, causes a larger deviation of the + signs in Figure 5 from a smooth curve. Data on $a_{C_N^0}$ obtained at the three different temperatures show no significant trend with changing temperature; any temperature dependence that may exist is less than the scatter in the data.

Comparing Figures 4 and 5 also shows that the empirical coefficient at any wavenumber is much greater for self broadening than for N_2 broadening. For example, at 400 cm^{-1}, $a_{C_S^0} = 6.6 \times 10^{-21}$ molecules^{-1} cm atm^{-1}, whereas $a_{C_N^0}$ is only 5.7×10^{-23} in the same units. The empirical continuum for N_2 broadening becomes almost negligible if bound is increased in the calculations; that is, if more distant lines are included when calculating the value that is subtracted from the experimental continuum. Thus, in much of this spectral region, the transmittance of room temperature samples can be calculated with reasonable accuracy by assuming the simple Lorentz line shape and summing the contributions due to all the lines. Farmer[20] has found this to be true, while also showing that the VVW shape predicts too much absorption for dilute samples of H_2O in N_2 if all lines are included. These results should not be taken as proof of the general validity of the simple Lorentz shape; it predicts far more absorption than is observed between 800 cm^{-1} and 1200 cm^{-1}.

---

[19] D. E. Burch and D. A. Gryvnak, AFGL-TR-0054, Final Report, Contract F19628-76-C-0302 (1979).

[20] B. Farmer, E.M.I. Electronics Ltd., Middlesex, England, Contract No. KH-G-5828-CB19(d)3 (1967).

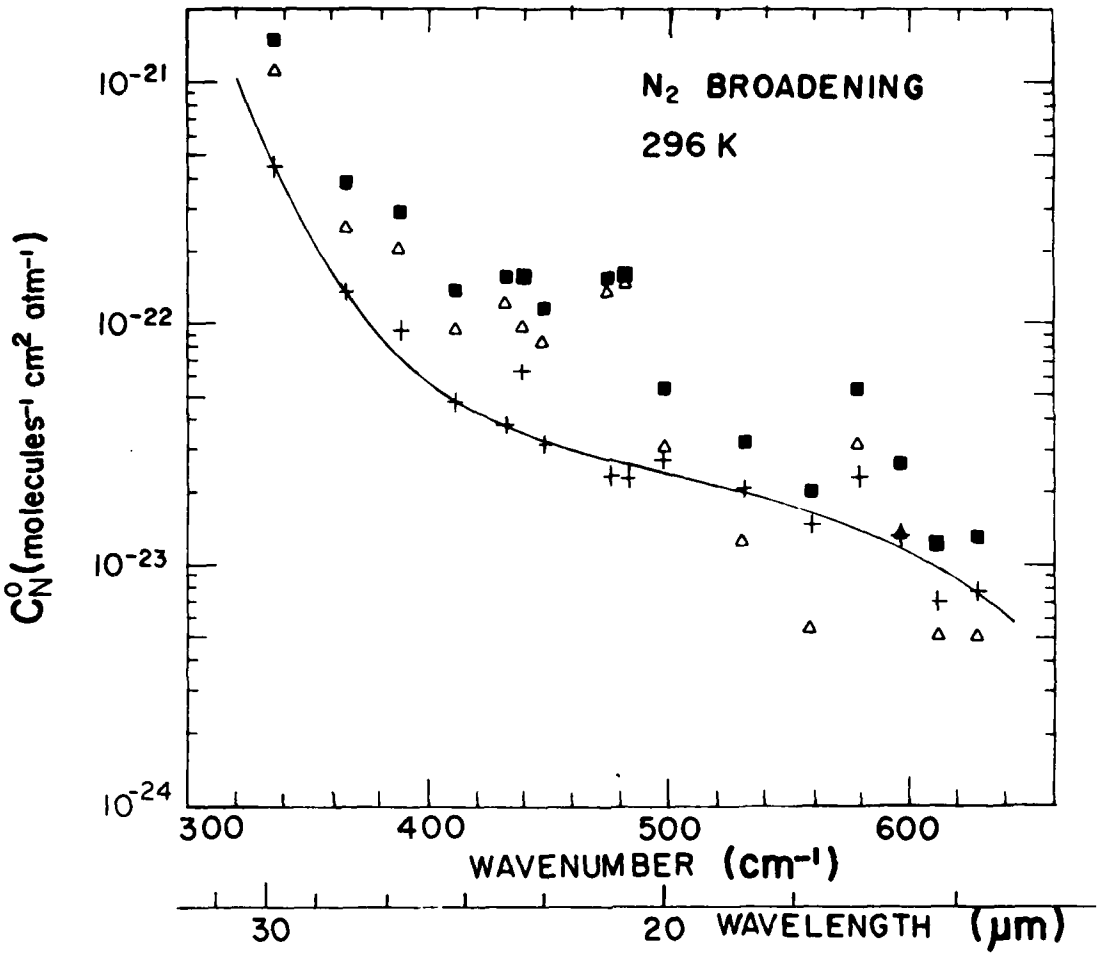

Figure 5. Semi-logarithmic plot of the H_2O continuum coefficient for N_2 broadening at 296 K. The symbols have the same meanings as in Figure 4.

Figure 6 illustrates the strong temperature dependence of the self broadening coefficient $^{a}C_{s}^{o}$. The solid curves are drawn over spectral regions for which experimental data are available. The broken curves are extrapolations based on the assumption that at a given wavenumber the coefficient varies in proportion to exp (-Constant/θ). Throughout the entire spectral interval, the value for 430 K is less than 0.3 of the corresponding value at 296 K. This dependence on temperature is much too strong to be due solely to decreases in the halfwidths of absorption lines that maintain a constant shape as the halfwidth changes.

The validity of this method of determining and using an empirical continuum has been demonstrated by calculating entire spectra with many fine spectral features and comparing the results with experimental spectra. In calculating a spectrum, the AFGL[1] line parameters are used to calculate the absorption coefficient due to the lines. Lines for which $| \nu - \nu_o | \leq 1$ are included, and the apodized bound of 30 cm^{-1} is employed. The appropriate empirical continuum coefficient is then included and the values of true transmittance T' are calculated for the sample parameters of interest. The spectrum is then "degraded" to account for the nonzero experimental spectral slitwidth so that the spectrum is directly comparable with the experimental spectra. The dots in Figure 3 represent values calculated in this manner for the sample represented by the solid curve. The agreement between the calculated and observed spectra is quite good. All the spectral structure that was observed, other than that obviously due to impurities, can be explained in terms of the H_2O lines. The important contribution by the empirical continuum is illustrated by the broken smooth curve in Figure 3.

Good agreement between calculated and experimental spectra was also observed for samples at elevated temperature and for samples of H_2O + N_2 when both the empirical continuum due to self-broadening and that due N_2-broadening were taken into account. The good agreement could not be obtained for all samples by simply adjusting the widths and intensities of the lines.

1250 cm^{-1} TO 2200 cm^{-1}

This spectral interval contains many very strong absorption lines that make up the ν_2 vibration-rotation band of H_2O vapor. This region is bounded on both sides by wide windows, and essentially all of the absorption arises from the lines centered within the spectral interval. Thus, the uncertainties in the contributions by the extreme wings of the lines centered at much lower wavenumbers (0-1000 cm^{-1}) or higher wavenumbers (2900-10,000 cm^{-1}) are unimportant when interpreting the data in this interval. All of the line-by-line calculations were limited to approximately the strongest 6200 lines centered between 1000 and 2500 cm^{-1}.

Tables 2-5 summarize the experimental data and calculated values of the continuum coefficients at 308K, 322K, 353K and 408K. As was done in the 333-825 cm^{-1} region, data were obtained at wavenumbers of maximum transmittance in very narrow windows between lines. The footnotes in Table 2 apply to all 4 tables. The contributions due to lines centered within 1 cm^{-1} of the wavenumber of calculation are not included in either the experimental or calculated values. Columns b, d and f make it convenient to compare the MVVW and

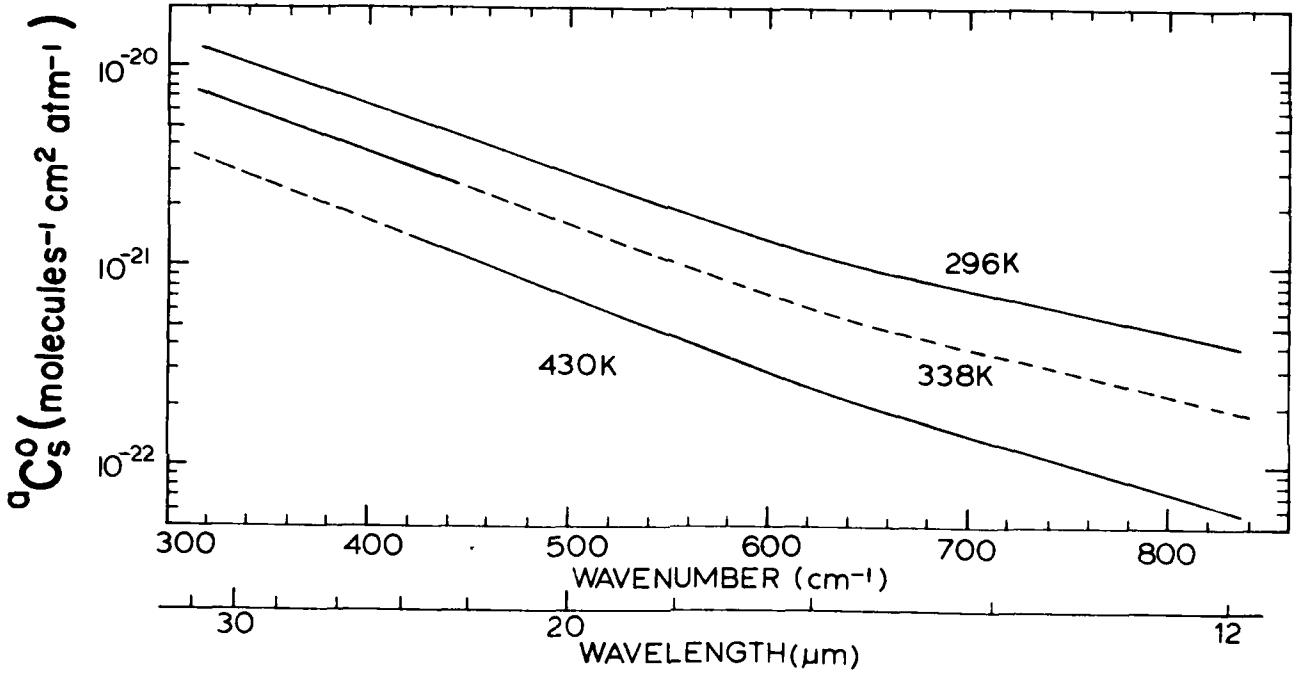

Figure 6. Semi-logarithmic plots of the empirical continuum coefficient for self broadening at 296 K, 338 K, and 430 K.

TABLE 2. CALCULATED, EXPERIMENTAL AND EMPIRICAL CONTINUUM (Temperature: 308 K)

a	b	c	d	e	f	g	h	i	j	k	l	m
	Calculated Values Based on AFGL Line Parameters $\left[\lvert \nu - \nu_0 \rvert > 1\ cm^{-1}\right]$							Experimental C^o		Empirical Continuum		
Wavenumber (cm^{-1})	N_2 Broadening					Self Broadening				Self Broadening		N_2 Br'd'g
	MVVW	MVVW Bound Apodized	Sim. Lor.	MVVW Fraction Beyond ≈25 cm^{-1}	Sim.Lor./MVVW	MVVW	Sim. Lor.	C_s^o	C_N^o	MVVW	Sim. Lor.	MVVW
1250.7	4.46E-24	1.46E-24	5.07E-24	6.22E-01	1.13E 00	2.03E-23	2.51E-23					
1275.5	9.89E-24	5.90E-24	1.05E-23	4.04E-01	1.04E 00	4.95E-23	5.25E-23					
1301.7	9.83E-24	4.31E-24	1.04E-23	5.84E-01	1.07E 00	4.93E-23	5.29E-23					
1331.1	3.70E-23	2.82E-24	3.29E-23	1.24E-01	1.03E 00	1.85E-22	1.89E-22					
1366.9	1.76E-22	1.61E-23	1.72E-22	8.11E-02	1.01E 00	8.78E-22	8.83E-22					
1413.6	2.23E-21	2.01E-22	2.24E-21	9.95E-02	1.01E 00	1.11E-21	1.12E-21	2.25E-21	3.15E-22	1.14E-21	1.13E-21	9.20E-23
1443.5	2.44E-21	2.13E-22	2.45E-21	1.26E-01	1.01E 00	1.22E-21	1.23E-21	2.43E-21	4.35E-22	1.21E-21	1.20E-21	1.91E-22
1479.7	4.91E-21	4.37E-22	4.91E-21	9.84E-02	1.00E 00	2.45E-21	2.46E-21	4.95E-21	8.03E-22	4.40E-21	4.39E-21	3.11E-22
1530.3	1.35E-21	1.22E-21	1.35E-21	4.25E-02	1.00E 00	6.73E-21	6.73E-21	1.32E-20	1.57E-21	6.97E-21	6.97E-21	5.83E-22
1584.0	2.47E-21	1.90E-22	2.45E-21	2.69E-01	9.95E-01	1.23E-21	1.23E-21	4.29E-21	4.23E-22	2.99E-21	2.99E-21	1.80E-22
1630.5	6.85E-22	6.38E-22	6.96E-22	6.83E-02	1.00E 00	3.42E-21	3.43E-21	8.64E-21	1.04E-21	5.22E-21	5.21E-21	3.55E-22
1665.5	9.72E-22	9.20E-22	9.72E-22	5.34E-02	9.99E-01	4.86E-21	4.86E-21	1.00E-20	1.36E-21	5.14E-21	5.14E-21	3.88E-22
1691.5	1.31E-21	1.26E-21	1.31E-21	3.85E-02	1.00E 00	6.55E-21	6.54E-21	1.19E-20	1.82E-21	5.35E-21	5.36E-21	5.11E-22
1725.2	4.63E-22	4.09E-22	4.61E-22	1.15E-01	9.97E-01	2.31E-21	2.31E-21	6.77E-21	7.23E-22	4.46E-21	4.72E-21	2.60E-22
1765.0	4.93E-22	4.55E-22	4.92E-22	7.71E-02	9.97E-01	2.46E-21	2.46E-21	5.35E-21	6.88E-22	2.89E-21	2.89E-21	1.95E-22
1786.5	3.33E-22	3.06E-22	3.32E-22	8.19E-02	9.97E-01	1.67E-21	1.66E-21	3.42E-21	4.25E-22	1.75E-21	1.76E-21	9.19E-23
1814.5	1.25E-22	1.02E-22	1.24E-22	1.83E-01	9.91E-01	6.25E-22	6.19E-22	1.89E-21	1.90E-22	1.27E-21	1.27E-21	6.50E-23
1839.8	2.07E-22	1.91E-22	2.06E-22	7.82E-02	9.96E-01	1.04E-21	1.03E-21	2.16E-21	2.97E-22	1.12E-21	1.13E-21	8.98E-23
1854.6	6.30E-23	4.88E-23	6.20E-23	2.24E-01	9.85E-01	3.15E-22	3.10E-22					
1882.0	4.58E-23	3.45E-23	4.50E-23	2.47E-01	9.83E-01	2.29E-22	2.25E-22					
1900.0	3.46E-23	2.49E-23	3.38E-23	2.81E-01	9.78E-01	1.73E-22	1.69E-22					
1905.6	6.66E-23	5.81E-23	6.60E-23	1.28E-01	9.90E 01	3.33E-22	3.30E-22					
1920.5	2.06E-22	1.98E-22	2.05E-22	3.72E-02	9.96E-01	1.03E-21	1.02E-21					
1927.1	4.27E-23	3.59E-23	4.19E-23	1.58E-01	9.82E-01	2.13E-22	2.10E-22					
1929.2	2.81E-23	2.15E-23	2.74E-23	2.34E-01	9.74E-01	1.40E-22	1.37E-22					
1931.3	2.77E-23	2.12E-23	2.70E-23	2.34E-01	9.75E-01	1.38E-22	1.35E-22					
1948.2	4.37E-23	3.74E-23	4.30E-23	1.44E-01	9.84E-01	2.19E-22	2.15E-22					
1952.6	2.01E-23	1.41E-23	1.95E-23	2.99E-01	9.68E-01	1.01E-22	9.75E-23					
1959.0	1.96E-23	1.41E-23	1.90E-23	2.81E-01	9.69E-01	9.81E-23	9.50E-23					
1962.8	2.73E-23	2.20E-23	2.67E-23	1.93E-01	9.78E-01	1.36E-22	1.33E-22					

TABLE 2. (Continued)

a	b	c	d	e	f	g	h
1974.0	1.12E-23	6.29E-24	1.06E-23	4.39E-01	9.47E-01	5.60E-23	5.30E-23
1978.5	8.87E-24	4.24E-24	8.29E-24	5.22E-01	9.35E-01	4.43E-23	4.15E-23
1983.8	1.17E-23	7.39E-24	1.12E-23	3.71E-01	9.53E-01	5.88E-23	5.60E-23
1990.0	7.98E-23	7.56E-23	7.93E-23	5.25E-02	9.93E-01	3.99E-22	3.96E-22
1997.4	1.95E-23	1.56E-23	1.89E-23	2.01E-01	9.72E-01	9.75E-23	9.47E-23
2002.3	8.62E-24	4.94E-24	8.08E-24	4.27E-01	9.37E-01	4.31E-23	4.04E-23
2006.4	1.28E-23	9.26E-24	1.23E-23	2.76E-01	9.59E-01	6.39E-23	6.13E-23
2008.8	1.60E-23	1.26E-23	1.55E-23	2.16E-01	9.67E-01	8.02E-23	7.75E-23
2011.8	9.38E-24	5.97E-24	8.87E-24	3.64E-01	9.45E-01	4.69E-23	4.43E-23
2029.3	5.85E-24	2.75E-24	5.35E-24	5.30E-01	9.15E-01	2.93E-23	2.68E-23
2036.1	5.91E-24	2.98E-24	5.43E-24	4.96E-01	9.18E-01	2.96E-23	2.71E-23
2045.3	1.17E-23	8.91E-24	1.12E-23	2.40E-01	9.59E-01	5.86E-23	5.62E-23
2055.5	3.74E-24	1.14E-24	3.28E-24	6.95E-01	8.77E-01	1.87E-23	1.64E-23
2056.0	3.81E-24	1.22E-24	3.35E-24	6.80E-01	8.79E-01	1.90E-23	1.67E-23
2071.1	4.09E-24	1.73E-24	3.65E-24	5.78E-01	8.91E-01	2.05E-23	1.82E-23
2083.6	3.28E-24	1.10E-24	2.85E-24	6.65E-01	8.68E-01	1.64E-23	1.42E-23
2102.4	2.59E-24	6.02E-25	2.18E-24	7.68E-01	8.40E-01	1.30E-23	1.09E-23
2109.6	2.39E-24	4.80E-25	1.99E-24	8.00E-01	8.30E-01	1.20E-23	9.93E-24
2130.7	1.96E-24	3.30E-25	1.57E-24	8.83E-01	8.01E-01	9.80E-24	7.85E-24
2133.0	2.17E-24	4.55E-25	1.78E-24	7.90E-01	8.21E-01	1.08E-23	8.90E-24
2169.8	1.73E-24	2.59E-25	1.37E-24	8.50E-01	7.91E-01	8.66E-24	6.85E-24
2196.7	1.41E-24	7.87E-26	1.07E-24	9.44E-01	7.56E-01	7.05E-24	5.33E-24
2223.3	1.29E-24	7.47E-26	9.61E-25	9.42E-01	7.45E-01	6.45E-24	4.80E-24
2290.0	1.08E-24	8.06E-26	7.78E-25	9.25E-01	7.23E-01	5.38E-24	3.89E-24

All coefficients have units of molecules^{-1} cm^{2} atm^{-1}. Data in the various columns of Tables 2-5 are as follows:

a. Wavenumber at which the continuum was calculated by line-by-line methods. Experimental data were also obtained at the wavenumbers indicated in columns i and j.

b-f. Calculated continuum based on the AFGL line parameters for N_2 broadening at a total pressure of 1 atm. Only lines for which $|\nu - \nu_0| > 1$ cm^{-1} are included in the calculation. Columns b and c are based on the MVVW shape, and d on the simple Lorentz shape. Column f gives the ratio of the calculated value based on the simple Lorentz shape to the value based on the MVVW shape. The values in columns b and d represent the sums of all of the contributions by the approximately 6200 most intense lines centered between 1000 cm-1 and 2500 cm-1. The values in column c were determined by using the 20-30 cm-1 apodized bound discussed above in the section on the 333 cm-1 to 825 cm-1 region. Each value in column e equals (b-c)/b, where b and c are the corresponding values in columns b and c. Thus, the value in e is approximately the fraction of the calculated coefficient due to lines centered beyond 25 cm^{-1}.

g,h. Columns g and h represent the calculated values for self broadening; each value is equal to 5 times the corresponding value in column b or c, respectively (see Equation (6)).

i,j These columns give the experimental data for the normalized continuum absorption coefficients for self broadening and N_2 broadening.

k-m. The normalized empirical continuum coefficients are found by subtracting each calculated value from the corresponding experimental value. For example, a value in column k equals the difference between the corresponding values in columns i and g.

TABLE 3. CALCULATED, EXPERIMENTAL AND EMPIRICAL CONTINUUM (Temperature:322 K)

a	b	c	d	e	f	g	h	i	j	k	l
	Calculated Values Based on AFGL Line Parameters $\left[\lvert \nu - \nu_0 \rvert > 1\ cm^{-1}\right]$							Experimental C°		Empirical Continuum	
Wavenumber (cm^{-1})	N_2 Broadening					Self Broadening				Self Broadening	
	MVVW	MVVW Bound Apodized	Sim. Lor.	MVVW Fraction Beyond ≈25 cm^{-1}	Sim.Lor./MVVW	MVVW	Sim. Lor.	C_S^o	C_N^o	MVVW	Sim. Lor.
1630.5	6.36E-22	5.91E-22	6.36E-22	7.00E-02	1.00E 00	3.18E-21	3.18E-21				
1665.5	9.12E-22	8.63E-22	9.11E-22	5.41E-02	9.99E-01	4.56E-21	4.56E-21				
1691.5	1.25E-21	1.21E-21	1.25E-21	3.83E-02	1.00E 00	6.27E-21	6.27E-21				
1725.2	4.54E-22	4.03E-22	4.53E-22	1.13E-01	9.97E-01	2.27E-21	2.26E-21				
1765.0	4.88E-22	4.51E-22	4.87E-22	7.51E-02	9.98E-01	2.44E-21	2.43E-21				
1786.5	3.41E-22	3.15E-22	3.40E-22	7.78E-02	9.97E-01	1.71E-21	1.70E-21				
1814.5	1.27E-22	1.05E-22	1.26E-22	1.75E-01	9.92E-01	6.34E-22	6.28E-22				
1839.8	2.06E-22	1.90E-22	2.05E-22	7.69E-02	9.96E-01	1.03E-21	1.02E-21				
1854.6	6.30E-23	4.92E-23	6.20E-23	2.19E-01	9.85E-01	3.15E-22	3.10E-22				
1382.0	4.58E-23	3.48E-23	4.51E-23	2.42E-01	9.83E-01	2.29E-22	2.25E-22	7.24E-22		4.95E-22	4.99E-22
1900.0	3.53E-23	2.58E-23	3.46E-23	2.70E-01	9.79E-01	1.77E-22	1.73E-22	6.19E-22		4.42E-22	4.46E-22
1905.6	6.70E-23	5.86E-23	6.63E-23	1.25E-01	9.90E-01	3.35E-22	3.32E-22	8.08E-22		4.73E-22	4.76E-22
1920.5	2.12E-22	2.04E-22	2.11E-22	3.55E-02	9.97E-01	1.06E-21	1.05E-21	1.90E-21		8.42E-22	8.45E-22
1927.1	4.40E-23	3.74E-23	4.33E-23	1.50E-01	9.83E-01	2.20E-22	2.16E-22	6.54E-22		4.34E-22	4.38E-22
1929.2	2.90E-23	2.25E-23	2.83E-23	2.22E-01	9.76E-01	1.45E-22	1.41E-22	4.78E-22		3.33E-22	3.37E-22
1931.3	2.90E-23	2.26E-23	2.83E-23	2.19E-01	9.77E-01	1.45E-22	1.41E-22	4.88E-22		3.43E-22	3.47E-22
1948.2	4.39E-23	3.76E-23	4.32E-23	1.42E-01	9.85E-01	2.19E-22	2.16E-22	5.14E-22		2.95E-22	2.98E-22
1952.6	2.08E-23	1.48E-23	2.01E-23	2.86E-01	9.70E-01	1.04E-22	1.01E-22	2.84E-22		1.80E-22	1.83E-22
1959.0	2.07E-23	1.53E-23	2.01E-23	2.62E-01	9.71E-01	1.04E-22	1.01E-22	3.42E-22		2.38E-22	2.41E-22
1962.8	2.85E-23	2.33E-23	2.79E-23	1.83E-01	9.80E-01	1.42E-22	1.39E-22	3.92E-22		2.50E-22	2.53E-22

TABLE 3. (Continued)

a	b	c	d	e	f	g	h	i	j	k	l
1974.0	1.15E-23	6.66E-24	1.09E-23	4.21E-01	9.50E-01	5.75E-23	5.46E-23	2.04E-22		1.47E-22	1.49E-22
1978.5	9.05E-24	4.49E-24	8.49E-24	5.03E-01	9.39E-01	4.52E-23	4.25E-23	1.90E-22		1.45E-22	1.48E-22
1983.8	1.23E-23	8.00E-24	1.18E-23	3.49E-01	9.57E-01	6.15E-23	5.88E-23	2.18E-22		1.57E-22	1.59E-22
1990.0	8.57E-23	8.16E-23	8.52E-23	4.82E-02	9.94E-01	4.28E-22	4.26E-22	9.05E-22		4.77E-22	4.79E-22
1997.4	2.00E-23	1.61E-23	1.94E-23	1.93E-01	9.73E-01	9.98E-23	9.71E-23	2.22E-22		1.22E-22	1.25E-22
2002.3	8.87E-24	5.26E-24	8.35E-24	4.07E-01	9.41E-01	4.44E-23	4.17E-23	1.57E-22		1.13E-22	1.15E-22
2006.4	1.38E-23	1.04E-23	1.33E-23	2.50E-01	9.63E-01	6.92E-23	6.66E-23	1.72E-22		1.03E-22	1.05E-22
2008.8	1.76E-23	1.42E-23	1.71E-23	1.92E-01	9.71E-01	8.82E-23	8.56E-23	3.30E-22		2.42E-22	2.44E-22
2011.8	9.87E-24	6.52E-24	9.37E-24	3.39E-01	9.50E-01	4.93E-23	4.69E-23	1.72E-22		1.23E-22	1.25E-22
2029.3	6.01E-24	2.97E-24	5.53E-24	5.07E-01	9.20E-01	3.01E-23	2.76E-23	1.05E-22		7.49E-23	7.74E-23
2036.1	6.30E-24	3.42E-24	5.83E-24	4.57E-01	9.26E-01	3.15E-23	2.92E-23	1.10E-22		7.85E-23	8.08E-23
2045.3	1.25E-23	9.71E-24	1.20E-23	2.21E-01	9.63E-01	6.23E-23	6.00E-23	1.37E-22		7.47E-23	7.70E-23
2055.5	3.84E-24	1.29E-24	3.39E-24	6.65E-01	8.84E-01	1.92E-23	1.70E-23	7.25E-23		5.33E-23	5.55E-23
2056.0	3.90E-24	1.36E-24	3.45E-24	6.52E-01	8.86E-01	1.95E-23	1.73E-23	7.48E-23		5.53E-23	5.75E-23
2071.1	4.23E-24	1.92E-24	3.80E-24	5.47E-01	8.98E-01	2.13E-23	1.90E-23	7.05E-23		4.93E-23	5.15E-23
2083.6	3.42E-24	1.29E-24	3.00E-24	[illegible]	8.78E-01	1.71E-23	1.50E-23	5.93E-23		4.22E-23	4.43E-23
2102.4	2.61E-24	6.68E-25	2.21E-24	[illegible]	8.46E-01	1.30E-23	1.10E-23	3.50E-23		2.20E-23	2.40E-23
2109.6	2.43E-24	5.67E-25	2.04E-24	[illegible]	8.38E-01	1.22E-23	1.02E-23	4.79E-23		3.57E-23	3.77E-23
2130.7	1.96E-24	2.72E-25	1.58E-24	[illegible]	8.08E-01	9.78E-24	7.90E-24	3.71E-23		2.73E-23	2.93E-23
2133.0	2.21E-24	5.41E-25	1.83E-24	[illegible]	8.30E-01	1.10E-23	9.16E-24	3.82E-23		2.72E-23	2.90E-23
2169.8	1.71E-24	2.84E-25	1.36E-24	8.34E-01	7.96E-01	8.57E-24	6.82E-24	2.51E-23		1.65E-23	1.83E-23
2196.7	1.39E-24	9.92E-26	1.06E-24	[illegible]	7.60E-01	6.95E-24	5.29E-24	2.32E-23		1.62E-23	1.79E-23
2223.3	1.27E-24	9.53E-26	9.55E-25	[illegible]	7.50E-01	6.37E-24	4.77E-24	2.00E-23		1.36E-23	1.52E-23
2290.0	1.08E-24	1.12E-25	7.88E-25	[illegible]	7.32E-01	5.38E-24	3.94E-24	1.79E-23		1.25E-23	1.40E-23

TABLE 4. CALCULATED, EXPERIMENTAL AND EMPIRICAL CONTINUUM (Temperature: 353 K)

a	b	c	d	e	f	g	h	i	j	k	l	m
	Calculated Values Based on AFGL Line Parameters					$\left[\lvert \nu - \nu_o \rvert > 1\ cm^{-1}\right]$		Experimental C^o		Empirical Continuum		
		N_2 Broadening				Self Broadening				Self Broadening		N_2 Br'd'g
Wavenumber (cm^{-1})	MVVW	MVVW Bound Apodized	Sim. Lor.	MVVW Fraction Beyond $\approx 25\ cm^{-1}$	Sim.Lor. / MVVW	MVVW	Sim. Lor.	C_s^o	C_N^o	MVVW	Sim. Lor.	MVVW
1250.7	5.17E-24	5.13E-24	5.20E-24	5.87E-01	1.10E 00	2.58E-23	2.85E-23	8.63E-23	4.08E-24	6.05E-23	5.[illegible]	[illegible]
1275.5	1.28E-23	8.46E-24	1.33E-23	3.79E-01	1.04E 00	6.39E-23	6.67E-23	1.44E-22	1.31E-23	8.29E-23	[illegible]	[illegible]
1301.7	1.27E-23	6.94E-24	1.34E-23	4.55E-01	1.05E 00	6.57E-23	6.71E-23	1.44E-22	2.63E-24	1.00E-22	9.[illegible]	[illegible]
1331.1	5.16E-23	4.29E-23	5.24E-23	1.68E-01	1.02E 00	2.58E-22	2.62E-22	3.78E-22	5.09E-23	1.20E-22	[illegible]	[illegible]
1366.9	2.10E-22	1.95E-22	2.10E-22	6.94E-02	1.00E 00	1.05E-21	1.05E-21	1.36E-21	2.42E-22	3.17E-22	[illegible]	[illegible]
1413.6	2.41E-22	2.20E-22	2.43E-22	8.89E-02	1.01E 00	1.21E-21	1.21E-21	2.06E-21	3.39E-22	8.53E-22	[illegible]	[illegible]
1443.5	2.47E-22	2.17E-22	2.48E-22	1.19E-01	1.00E 00	1.24E-21	1.24E-21	2.55E-21	3.90E-22	1.33E-21	[illegible]	[illegible]
1479.7	4.90E-22	4.44E-22	4.91E-22	9.14E-02	1.00E 00	2.45E-21	2.44E-21					
1530.3	1.32E-21	1.07E-21	1.32E-21	3.77E-02	1.00E 00	6.60E-21	6.60E-21					
1584.0	2.02E-22	1.44E-22	2.01E-22	2.85E-01	9.94E-01	1.01E-21	1.00E-21					
1630.5	5.44E-22	5.04E-22	5.45E-22	7.37E-02	1.00E 00	2.72E-21	2.72E-21	5.04E-21	8.71E-22	2.32E-21	2.[illegible]	3.[illegible]
1665.5	7.98E-22	7.54E-22	7.98E-22	5.54E-02	1.00E 00	3.99E-21	3.99E-21	6.12E-21	1.10E-21	2.13E-21	2.[illegible]	3.03E-22
1691.5	1.14E-21	1.10E-21	1.14E-21	3.78E-02	1.00E 00	5.72E-21	5.72E-21	8.41E-21	1.50E-21	2.69E-21	2.[illegible]	3.55E-22
1725.2	4.35E-22	3.89E-22	4.34E-22	1.07E-01	9.97E-01	2.18E-21	2.17E-21	4.25E-21	6.96E-22	2.07E-21	2.[illegible]	2.61E-22
1765.0	4.75E-22	4.41E-22	4.74E-22	7.14E-02	9.98E-01	2.38E-21	2.37E-21	4.57E-21	6.95E-22	2.19E-21	2.[illegible]	2.20E-22
1786.5	3.59E-22	3.34E-22	3.58E-22	6.99E-02	9.97E-01	1.79E-21	1.79E-21	2.81E-21	4.19E-22	1.02E-21	1.[illegible]	6.04E-23
1814.5	1.31E-22	1.10E-22	1.30E-22	1.59E-01	9.93E-01	6.54E-22	6.49E-22	1.49E-21	1.95E-22	8.36E-22	8.[illegible]	6.42E-23
1839.8	2.02E-22	1.87E-22	2.01E-22	7.44E-02	9.97E-01	1.01E-21	1.01E-21	1.78E-21	2.83E-22	7.71E-22	7.[illegible]	8.11E-23
1854.6	6.29E-23	4.98E-23	6.20E-23	2.09E-01	9.86E-01	3.15E-22	3.10E-22	8.45E-22	9.00E-23	5.30E-22	5.[illegible]	2.71E-23
1882.0	4.59E-23	3.53E-23	4.52E-23	2.31E-01	9.85E-01	2.29E-22	2.26E-22	5.60E-22	5.80E-23	3.31E-22	3.[illegible]	1.21E-23
1900.0	3.70E-23	2.79E-23	3.63E-23	2.47E-01	9.82E-01	1.85E-22	1.82E-22					
1905.6	6.73E-23	5.93E-23	6.67E-23	1.19E-01	9.91E-01	3.36E-22	3.33E-22	6.00E-22	9.15E-23	2.64E-22	2.[illegible]	2.42E-23
1920.5	2.22E-22	2.14E-22	2.21E-22	3.25E-02	9.97E-01	1.11E-21	1.10E-21					
1927.1	4.64E-23	4.00E-23	4.57E-23	1.36E-01	9.85E-01	2.32E-22	2.28E-22					
1929.2	3.08E-23	2.46E-23	3.01E-23	2.00E-01	9.79E-01	1.54E-22	1.51E-22	3.42E-22	4.10E-23	1.88E-22	1.[illegible]	1.02E-23
1931.3	3.16E-23	2.55E-23	3.10E-23	1.92E-01	9.80E-01	1.58E-22	1.55E-22	3.72E-22	3.77E-23	2.14E-22	2.[illegible]	5.12E-24
1948.2	4.39E-23	3.79E-23	4.33E-23	1.37E-01	9.86E-01	2.19E-22	2.16E-22					
1952.6	2.20E-23	1.62E-23	2.14E-23	2.62E-01	9.74E-01	1.10E-22	1.07E-22	2.47E-22	2.63E-23	1.37E-22	1.4[illegible]	4.29E-24
1959.0	2.34E-23	1.81E-23	2.28E-23	2.26E-01	9.76E-01	1.17E-22	1.14E-22					
1962.8	3.07E-23	2.56E-23	3.01E-23	1.65E-01	9.83E-01	1.53E-22	1.51E-22	2.83E-22	3.95E-23	1.30E-22	1.[illegible]	8.83E-24

TABLE 4. (Continued)

a	b	c	d	e	f	g	h	i	j	k	l	m	n
1974.0	1.21E-23	2.40E-24	1.15E-23	3.87E-01	9.56E-01	6.04E-23	5.77E-23						
1978.5	9.44E-24	5.03E-24	8.92E-24	4.66E-01	9.45E-01	4.72E-23	4.46E-23	1.44E-22	1.05E-23	9.58E-23	9.93E-23	3.06E-24	7.47E-24
1983.8	1.34E-23	9.28E-24	1.29E-23	3.09E-01	9.64E-01	6.71E-23	6.47E-23						
1990.0	9.74E-23	9.34E-23	9.69E-23	4.11E-02	9.95E-01	4.87E-22	4.85E-22						
1997.4	2.08E-23	1.71E-23	2.03E-23	1.78E-01	9.76E-01	1.04E-22	1.02E-22						
2002.3	9.44E-24	5.97E-24	8.95E-24	3.68E-01	9.48E-01	4.72E-23	4.48E-23						
2006.4	1.62E-23	1.28E-23	1.57E-23	2.05E-01	9.71E-01	8.08E-23	7.85E-23						
2008.8	2.12E-23	1.80E-23	2.07E-23	1.53E-01	9.77E-01	1.06E-22	1.04E-22						
2011.8	1.09E-23	7.67E-24	1.04E-23	2.94E-01	9.57E-01	5.44E-23	5.21E-23						
2029.3	6.40E-24	3.46E-24	5.94E-24	4.59E-01	9.29E-01	3.20E-23	2.97E-23	7.27E-23	6.30E-24	4.57E-23	4.80E-23	1.96E-25	2.74E-24
2036.1	7.24E-24	4.47E-24	6.80E-24	3.82E-01	9.40E-01	3.62E-23	3.40E-23						
2045.3	1.42E-23	1.15E-23	1.37E-23	1.88E-01	9.69E-01	7.08E-23	6.86E-23						
2055.5	4.08E-24	1.63E-24	3.67E-24	6.01E-01	8.98E-01	2.04E-23	1.83E-23						
2056.0	4.12E-24	1.67E-24	3.70E-24	5.94E-01	8.99E-01	2.06E-23	1.85E-23						
2071.1	4.57E-24	2.35E-24	4.17E-24	4.85E-01	9.12E-01	2.29E-23	2.08E-23	5.20E-23	4.50E-24	2.91E-23	3.12E-23	2.18E-26	2.15E-24
2083.6	3.77E-24	1.74E-24	3.39E-24	5.38E-01	8.97E-01	1.89E-23	1.69E-23	4.35E-23	3.80E-24	2.34E-23	2.56E-23	1.57E-26	2.06E-24
2102.4	2.67E-24	8.21E-25	2.29E-24	6.92E-01	8.60E-01	1.33E-23	1.15E-23						
2109.6	2.57E-24	7.95E-25	2.20E-24	6.91E-01	8.57E-01	1.28E-23	1.10E-23						
2130.7	1.98E-24	3.83E-25	1.63E-24	8.06E-01	8.32E-01	9.89E-24	8.13E-24	2.00E-23	1.70E-24	1.01E-23	1.19E-23	2.72E-27	1.33E-24
2133.0	2.33E-24	7.58E-25	1.98E-24	6.75E-01	8.50E-01	1.17E-23	9.93E-24						
2169.8	1.70E-24	3.49E-25	1.37E-24	7.95E-01	8.08E-01	8.49E-24	6.86E-24						
2196.7	1.37E-24	1.55E-25	1.06E-24	8.87E-01	7.73E-01	6.84E-24	5.29E-24	1.18E-23	5.80E-25	4.94E-24	4.57E-24	5.89E-28	4.25E-25
2223.3	1.26E-24	1.54E-25	9.63E-25	8.78E-01	7.64E-01	6.30E-24	4.81E-24						
2290.0	1.11E-24	2.10E-25	8.43E-25	8.11E-01	7.59E-01	5.56E-24	4.22E-24						

TABLE 5. CALCULATED, EXPERIMENTAL AND EMPIRICAL CONTINUUM (Temperature: 428 K)

a	b	c	d	e	f	g	h	i	j	k	l	m
	Calculated Values Based on AFGL Line Parameters					$\left[\lvert \nu - \nu_0 \rvert > 1\ cm^{-1}\right]$		Experimental C^o		Empirical Continuum		
Wavenumber (cm^{-1})	N_2 Broadening					Self Broadening				Self Broadening		N_2 Br'd'g
	MVVW	MVVW Bound Apodized	Sim. Lor.	MVVW Fraction Beyond $\pm 25\ cm^{-1}$	Sim.Lor. / MVVW	MVVW	Sim. Lor.	C_s^o	C_N^o	MVVW	Sim. Lor.	MVVW
1250.7	7.29E-24	4.11E-24	7.28E-24	4.37E-01	1.00E 00	3.65E-23	3.89E-23					
1273.5	1.95E-23	1.51E-23	1.90E-23	2.23E-01	1.03E 00	9.75E-23	1.00E-22	1.63E-22		6.29E-23	6.69E-23	
1301.7	1.89E-23	1.37E-23	1.95E-23	3.28E-01	1.03E 00	9.45E-23	9.73E-23	1.54E-22		5.99E-23	6.33E-23	
1331.1	7.65E-23	6.75E-23	7.73E-23	1.12E-01	1.01E 00	3.83E-22	3.83E-22	4.60E-22		2.48E-23	2.85E-23	
1366.9	2.49E-22	2.34E-22	2.49E-22	5.94E-02	1.00E 00	1.24E-21	1.25E-21	1.59E-21		3.47E-22	3.44E-22	
1413.6	2.60E-22	2.40E-22	2.61E-22	2.28E-02	1.00E 00	1.30E-21	1.31E-21	1.13E-21		8.29E-22	8.23E-22	
1443.5	2.47E-22	2.30E-22	2.48E-22	1.09E-01	1.00E 00	1.24E-21	1.24E-21	2.19E-21		8.52E-22	8.47E-22	
1479.7	4.82E-22	4.41E-22	4.84E-22	8.38E-02	1.00E 00	2.41E-21	2.41E-21					
1530.3	1.28E-21	1.24E-21	1.28E-21	3.18E-02	1.00E 00	6.39E-21	6.39E-21					
1584.0	1.53E-22	1.06E-22	1.52E-22	3.62E-01	9.94E-01	7.66E-22	7.62E-22					
1630.5	3.92E-22	3.60E-22	3.92E-22	8.20E-02	1.00E 00	1.96E-21	1.96E-21					
1665.5	6.02E-22	5.67E-22	6.02E-22	5.83E-02	1.00E 00	3.01E-21	3.01E-21					
1691.5	9.32E-22	8.97E-22	9.32E-22	3.75E-02	1.00E 00	4.66E-21	4.66E-21					
1725.2	3.92E-22	3.54E-22	3.91E-22	9.72E-02	9.98E-01	1.96E-21	1.96E-21					
1765.0	4.40E-22	4.11E-22	4.39E-22	6.50E-02	9.98E-01	2.20E-21	2.20E-21					
1786.5	3.90E-22	3.68E-22	3.89E-22	5.65E-02	9.98E-01	1.95E-21	1.94E-21					
1814.5	1.41E-22	1.22E-22	1.40E-22	1.31E-01	9.94E-01	7.03E-22	6.99E-22					
1839.8	1.94E-22	1.80E-22	1.93E-22	6.93E-02	9.97E-01	9.68E-22	9.66E-22					
1854.6	6.27E-23	5.09E-23	6.19E-23	1.88E-01	9.88E-01	3.13E-22	3.10E-22	5.83E-22	8.31E-23	2.70E-22	2.73E-22	2.04E-23
1882.0	4.64E-23	3.68E-23	4.58E-23	2.07E-01	9.87E-01	2.32E-22	2.29E-22	4.19E-22	5.70E-23	1.87E-22	1.90E-22	1.06E-23
1900.0	4.22E-23	3.39E-23	4.16E-23	1.97E-01	9.86E-01	2.11E-22	2.08E-22	3.71E-22		1.60E-22	1.63E-22	
1905.6	6.64E-23	5.91E-23	6.59E-23	1.09E-01	9.92E-01	3.32E-22	3.29E-22	4.88E-22	8.45E-23	1.56E-22	1.59E-22	1.81E-23
1920.5	2.32E-22	2.25E-22	2.31E-22	2.83E-02	9.98E-01	1.16E-21	1.16E-21	1.64E 21	2.96E-22	4.81E-22	4.84E-22	6.42E-23
1927.1	4.93E-23	4.36E-23	4.87E-23	1.16E-01	9.88E-01	2.47E-22	2.44E-22	4.33E-22		1.86E-22	1.89E-22	
1929.2	3.45E-23	2.89E-23	3.39E-23	1.63E-01	9.84E-01	1.72E-22	1.70E-22	2.81E-22	4.29E-23	1.09E-22	1.11E-22	8.42E-24
1931.3	3.69E-23	3.13E-23	3.63E-23	1.50E-01	9.86E-01	1.84E-22	1.82E-22	2.85E-22	4.64E-23	1.01E-22	1.03E-22	9.54E-24
1948.2	4.31E-23	3.75E-23	4.26E-23	1.29E-01	9.87E-01	2.16E-22	2.13E-22	3.44E-22		1.28E-22	1.31E-22	
1952.6	2.44E-23	1.90E-23	2.39E-23	2.20E-01	9.80E-01	1.22E-22	1.20E-22	1.99E-22	2.97E-23	7.69E-23	7.94E-23	5.29E-24
1959.0	3.06E-23	2.57E-23	3.02E-23	1.61E-01	9.84E-01	1.53E-22	1.51E-22	2.22E-22		6.88E-23	7.12E-23	
1962.8	3.40E-23	2.93E-23	3.36E-23	1.39E-01	9.87E-01	1.70E-22	1.68E-22	2.38E-22		6.78E-23	7.01E-23	

TABLE 5. (Continued)

a	b	c	d	e	f	g	h	i	j	k	l	m	n
1974.0	1.33E-23	8.99E-24	1.29E-23	3.26E-01	9.65E-01	6.67E-23	6.44E-23	1.18E-22	1.67E-23	5.13E-23	5.36E-23	3.34E-24	
1978.5	1.04E-23	6.27E-24	9.92E-24	3.95E-01	9.57E-01	5.18E-23	4.96E-23	1.08E-22	1.37E-23	5.62E-23	5.84E-23	3.34E-24	
1983.8	1.57E-23	1.18E-23	1.53E-23	2.46E-01	9.74E-01	7.86E-23	7.65E-23	1.39E-22		6.04E-23	6.25E-23		
1990.0	1.18E-22	1.14E-22	1.17E-22	3.19E-02	9.97E-01	5.89E-22	5.86E-22	7.66E-22	1.59E-23	1.77E-22	1.80E-22	4.13E-23	
1997.4	2.24E-23	1.89E-23	2.19E-23	1.55E-01	9.80E-01	1.12E-22	1.10E-22	1.64E-22	2.75E-23	5.22E-23	5.45E-23	5.15E-24	
2002.3	1.10E-23	7.81E-24	1.06E-23	2.91E-01	9.61E-01	5.50E-23	5.29E-23	9.31E-23		3.81E-23	4.02E-23		
2006.4	2.13E-23	1.83E-23	2.09E-23	1.43E-01	9.81E-01	1.07E-22	1.05E-22	1.39E-22		3.23E-23	3.43E-23		
2008.8	2.92E-23	2.62E-23	2.87E-23	1.02E-01	9.86E-01	1.46E-22	1.44E-22	2.72E-22		1.26E-22	1.28E-22		
2011.8	1.29E-23	9.93E-24	1.25E-23	2.31E-01	9.69E-01	6.46E-23	6.26E-23	1.32E-22		5.24E-23	5.94E-23		
2029.3	7.41E-24	4.70E-24	7.02E-24	3.67E-01	9.47E-01	3.71E-23	3.51E-23	6.18E-23		2.47E-23	2.67E-23		
2036.1	9.72E-24	7.16E-24	9.34E-24	2.63E-01	9.41E-01	4.86E-23	4.67E-23	8.07E-23	1.22E-23	3.21E-23	3.40E-23	2.48E-24	
2045.3	1.82E-23	1.57E-23	1.78E-23	1.36E-01	9.79E-01	9.11E-23	8.92E-23	1.25E-22		3.49E-23	3.58E-23		
2055.5	4.87E-24	2.59E-24	4.51E-24	4.68E-01	9.26E-01	2.44E-23	2.26E-23	4.04E-23	5.55E-24	1.60E-23	1.78E-23	4.13E-24	
2056.0	4.76E-24	2.50E-24	4.41E-24	4.76E-01	9.25E-01	2.38E-23	2.20E-23	3.91E-23		1.53E-23	1.71E-23		
2071.1	5.45E-24	3.40E-24	5.10E-24	3.76E-01	9.36E-01	2.73E-23	2.55E-23	4.31E-23	6.65E-24	1.58E-23	1.76E-23	1.30E-24	
2083.6	4.80E-24	2.95E-24	4.47E-24	3.86E-01	9.30E-01	2.40E-23	2.23E-23	3.78E-23		1.38E-23	1.55E-23		
2102.4	2.89E-24	1.21E-24	2.57E-24	5.82E-01	8.88E-01	1.45E-23	1.28E-23	2.02E-23		5.23E-24	7.35E-24		
2109.6	3.12E-24	1.51E-24	2.80E-24	5.17E-01	8.98E-01	1.56E-23	1.40E-23	2.26E-23	3.00E-24	7.00E-24	8.59E-24	-1.20E-25	
2130.7	2.17E-24	7.38E-25	1.87E-24	6.60E-01	8.60E-01	1.09E-23	9.34E-24	1.80E-23	1.90E-24	7.14E-24	8.66E-24	-2.10E-25	
2133.0	2.83E-24	1.41E-24	2.53E-24	5.00E-01	8.94E-01	1.41E-23	1.26E-23	2.11E-23		6.96E-24	8.46E-24		
2169.8	1.77E-24	5.67E-25	1.49E-24	6.80E-01	8.41E-01	8.83E-24	7.46E-24	8.80E-24	1.20E-24	-7.00E-26	1.34E-24	-1.40E-25	
2196.7	1.42E-24	3.44E-25	1.15E-24	7.58E-01	8.11E-01	7.10E-24	5.76E-24	7.00E-24	8.60E-25	-1.01E-25	1.24E-24	-1.60E-25	
2223.3	1.35E-24	3.71E-25	1.09E-24	7.24E-01	8.10E-01	6.73E-24	5.45E-24	6.90E-24		1.17E-24	2.45E-24		
2290.0	1.42E-24	6.32E-25	1.19E-24	5.55E-01	8.37E-01	7.11E-24	5.95E-24						

simple Lorentz line shapes (see Table 1). In the strong parts of the bands, the calculated coefficients are essentially the same for both of these line shapes. These values are also approximately the same as those in column c that were calculated by using the MVVW shape and the apodized bound. Thus, most of the calculated absorption at windows witnin the strong parts of the band is due to lines centered within approximately 25 cm^{-1}. Column e shows that this is not true in the narrow windows in the wings of the band from approximately 1250 to 1400 cm^{-1} and above 1800 cm^{-1}.

The continuum measurements for pure H_2O at 308K made within narrow windows in the strong part of the band are summarized graphically in Figure 7. These data were obtained[21] in a manner similar to that used for the narrow windows between lines from 333 cm^{-1} to 825 cm^{-1}. The circles represent values calculated by assuming the MVVW line shape. The empirical continuum represents a quantity somewhat different from the one designated by $^{a}C_{S}^{0}$ for the 330-825 cm^{-1} region because of the difference in the value of bound.

The shape of the empirical continuum curve drawn through the +'s in Figure 7 cannot be determined accurately because of the limited number of data points and the ± 5% to ± 8% uncertainty in the experimental data. However, the minimum near the center of the ν_2 band at 1595 cm^{-1} is real. The maxima of the curve near 1530 cm^{-1} and 1660 cm^{-1} occur near the strongest lines in the P and R branches of this band.

Some of the experimental values are more than twice the corresponding calculated values. Such large discrepancies have been observed by many workers in the wide windows of infrared and millimeter regions, but they have not previously been expected in the narrow windows within a strong vibration-rotation band.

Figure 8 contains a composite of the corresponding curves of the empirical continuum for self broadening and N_2 broadening at different temperatures. The two maxima and the minimum appear in the curve for N_2 broadening as well as in the one for self broadening repeated from Figure 7. This provides further evidence that the structure in the empirical continuum is real. Two important features of the curves, similar to the corresponding curves for the 333-835 cm^{-1} region, are apparent. There is a very strong negative temperature dependence, and the self-broadening coefficients are much larger than the corresponding N_2-broadening coefficients.

Figure 9 compares the spectral curve of the empirical continuum for self broadening at 308K with a smooth curve (V) that is related directly to the average intensities of the H_2O vapor lines. To construct this curve, we calculated the sums of the intensities of the lines centered within 25 cm^{-1} intervals, and divided by 25. We then plotted these values with the points at the centers of the spectral intervals and drew the curve through the points with some extra smoothing of the curve. Note the strong similarity in the shapes of these two curves. The corresponding minimum and the maxima are essentially superimposed, and the decreases in the wings of the band are similar, although the decreases are somewhat more rapid in curve V.

[21] D. E. Burch, D. A. Gryvnak, and G. H. Piper, AFCRA-TR-73-0530, Final Report, Contract F19628-73-C-0011 (1973).

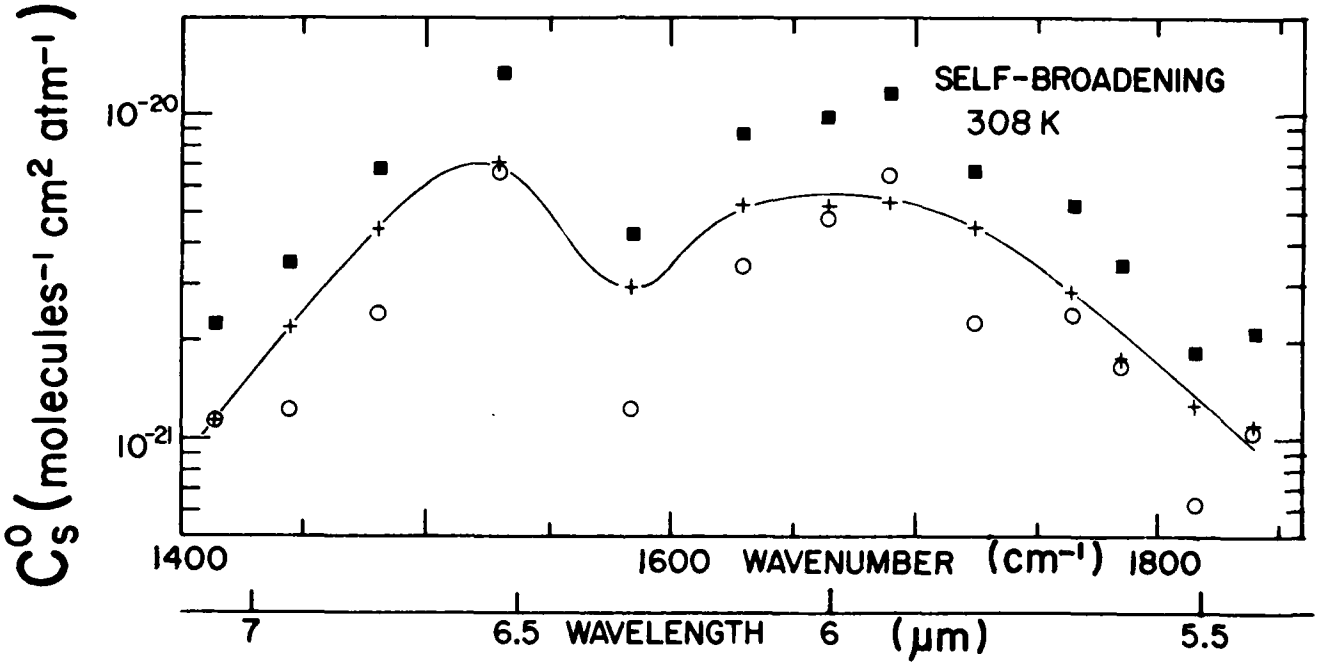

Figure 7. Spectral plot of the continuum coefficients for pure H_2O at 308 K. The empirical continuum curve is drawn through the +'s, which represent the differences between the experimental values (solid squares) and the calculated values based on the line parameters (circles).

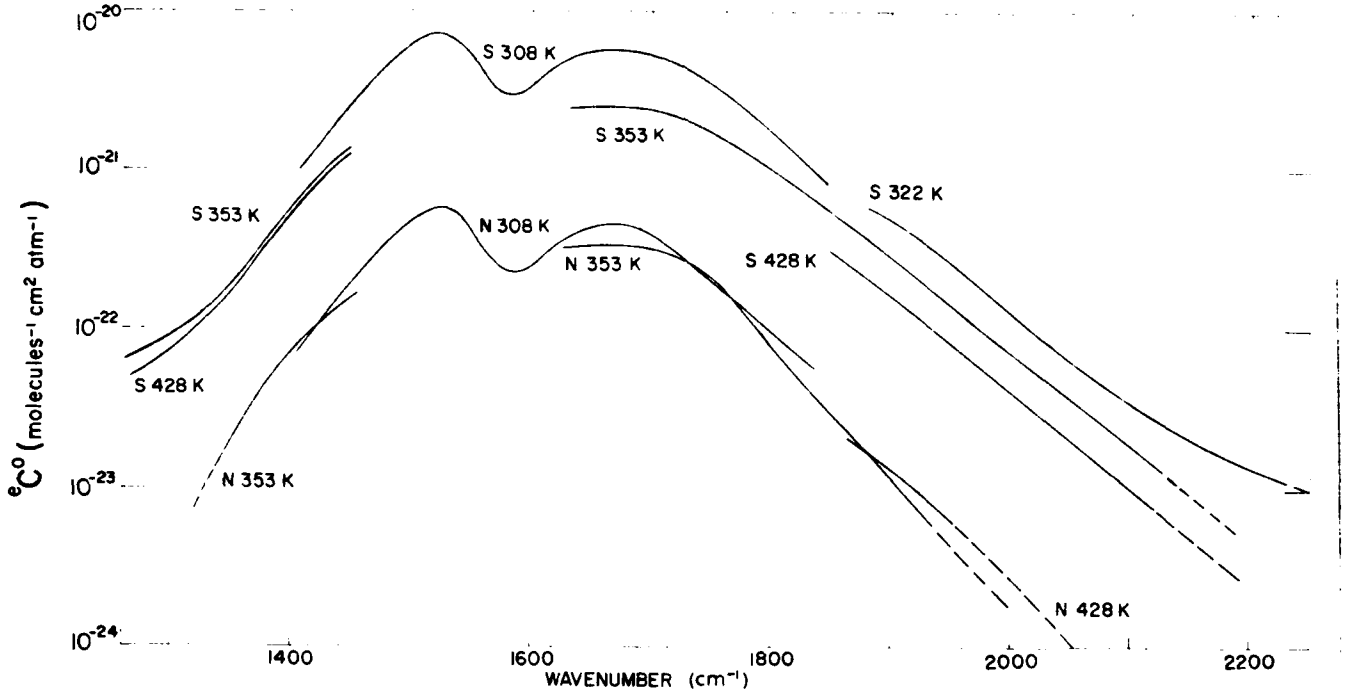

Figure 8. Composite of spectral curves of $^{e}C^{o}$ for self broadening and N_2 broadening at various temperatures. S denotes self broadening and N denotes N_2 broadening.

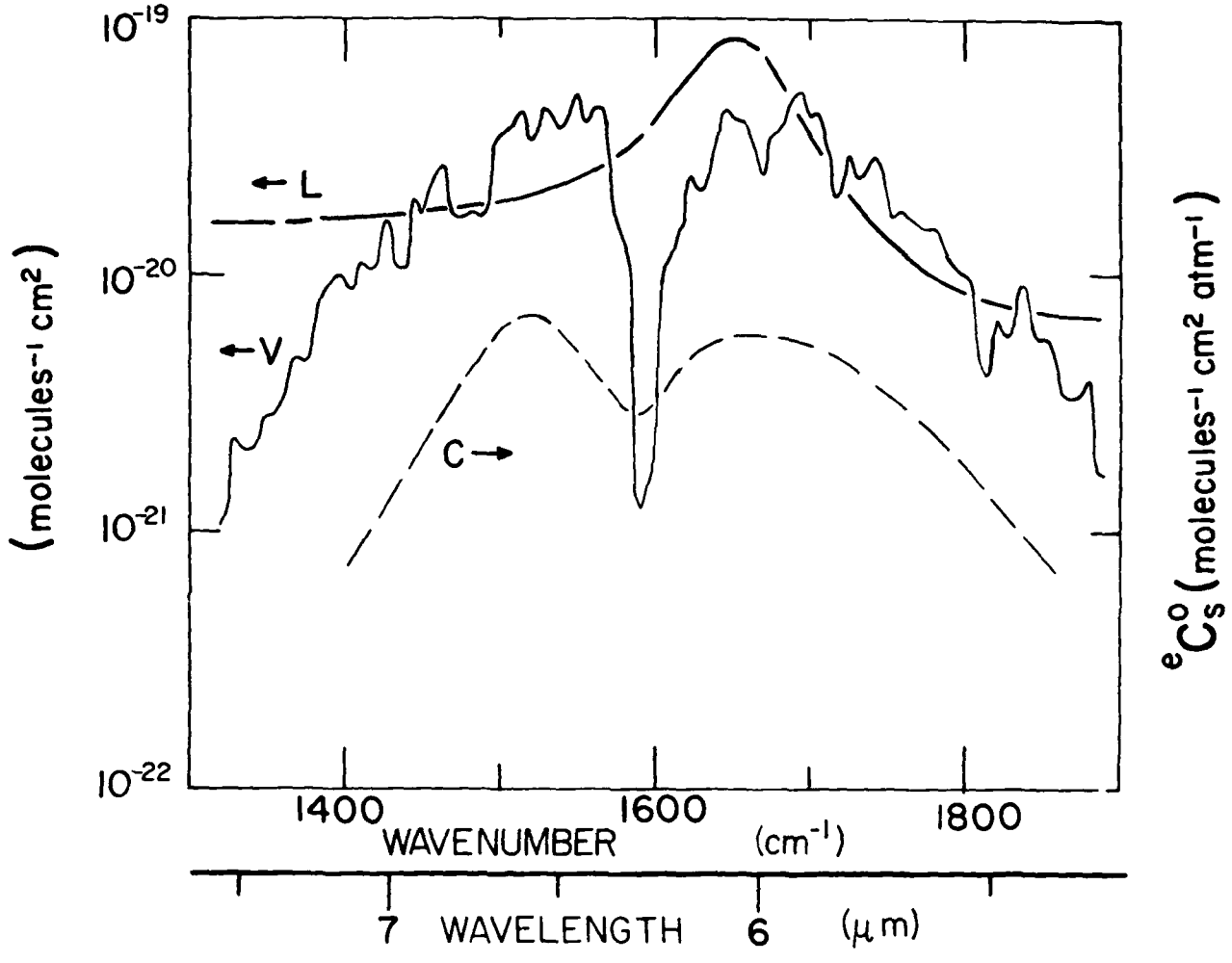

Figure 9. Comparison of the spectral curves between 1350 and 1850 cm^{-1} of the empirical continuum for self broadening (C), the absorption coefficient of liquid water (L), and the average intensities of the H_2O vapor lines (V).

The probability of a rotational transition for the absorption lines is greater near the maxima of curve V than it is near the center or the wings of the bands. The similarity in the shapes of curves C and V suggests that the excess absorption represented by the empirical continuum is associated directly with both the rotational transitions and the vibrational transition involved in the band. It seems unlikely that the empirical continuum would display the spectral characteristics it does if it were due to a completely different process that involves dimers made up of two bound H_2O molecules rotating as semi-rigid rotators or vibrating in a mode that involves relative motion between the two molecules. If the excess absorption is, in fact, due to dimers, the binding must be such that each H_2O molecule forming a dimer is still free to vibrate and rotate similar to the way it does in the normal monomer state. In such a case, at least some shifts would be expected in the vibrational and rotational frequencies. No significant shift is observable in Figure 9 between curves V and C.

Curve L, which represents the absorption coefficient for liquid water[22], shows a maximum with no fine structure in this region. This maximum is to be expected because liquids generally display absorption maxima in the same spectral regions as does the vapor of the same compound. However, two differences between curves L and V are significant. Curve L contains only a single maximum, and it is shifted approximately 60 cm^{-1} from the central minimum in curve V, which corresponds to the center of the ν_2 vibration-rotation band of the vapor. The strong similarity between curves V and C suggests that the empirical continuum is associated with vapor rather than liquid. Thus, this result is inconsistent with the suggestion that the excess absorption represented by the empirical continuum is due to liquid-like absorption by clusters of many water molecules. If the clusters were to take on the spectral characteristics of liquid and produce the excess absorption, the expected shape of the resulting empirical continuum curve would be more like curve L than curve V of Figure 9. This is obviously not the case.

The very significant effect of N_2, represented by the curves of $^{e}C^{o}_{N}$, suggests further that the excess absorption is associated directly with the vibration-rotation band rather than with dimers or clusters. Continuum absorption by dimers or clusters is expected to be essentially independent of the presence of nonabsorbing N_2. Thus, it seems likely that much of the excess absorption is due to the extreme wings of individual absorption lines that absorb more than is predicted by any of the widely used theoretical line shapes. Furthermore, the excess absorption where most of the calculated absorption is due to lines centered within 25 cm^{-1} (see column e of Tables 2-5) implies that much of the excess is due to the wings of lines within 25 cm^{-1} of their centers.

The uncertainty in the curves of Figure 8 increases from approximately ± 10% or 15% for $^{e}C^{o}$ greater than 10^{-21} $molecules^{-1}$ cm^2 atm^{-1} to as much as ±50% when $^{e}C^{o}$ has decreased to 10^{-23} $molecules^{-1}$ cm^2 atm^{-1}. The dashed parts of the curves indicate large uncertainties. At a few of the wavenumbers above 2000 cm^{-1}, the calculated values of $\sum k^{o}$ exceed the experimental values of C^{o}_{N} for N_2 broadening at the two higher temperatures. This apparent negative empirical continuum implies that the extreme wings of N_2-broadened lines are "sub-MVVW"; that is, they absorb less than lines of the MVVW shape with the same intensity and halfwidth. The relatively large uncertainty in these apparent negative values of $^{e}C^{o}$ makes it impossible to

[22] G. M. Hale and M. R. Querry, Appl. Opt. 12, 555 (1973)

confirm a sub-MVVW shape for the wings of N_2-broadened H_2O lines in this region. However, such a result is not surprising because the extremely weak dependence of the 800 cm^{-1} to 1200 cm^{-1} continuum on N_2 broadening indicates that the very extreme wings of the rotational lines are very much sub-MVVW. Thus, it is apparent that at some point in the wings, an N_2-broadened H_2O line becomes sub-MVVW. Because of the similarity between the shapes of MVVW lines and Lorentz lines in the infrared, the curves of Figure 8 would be very similar to what they are if the simple Lorentz shape had been used instead of the MVVW shape. The only significant changes would occur above 2000 cm^{-1}.

A quantitative interpretation of the obvious decrease in $^{e}C^{o}$ with increasing temperature is complicated by the shift in the intensities of the lines. As the temperature increases, the lines in the wings of the band increase in intensity at the expense of the lines closer to the band center (near 1595 cm^{-1}). This shift causes $^{e}C^{o}$ in the wings of the band to be higher at high temperatures than it would be if the lines remained constant in intensity while changing in shape and width.

MILLIMETER-WAVE AND MICROWAVE REGIONS

From approximately 36 cm^{-1} to 250 cm^{-1} (40 μm), absorption by the pure rotation lines of H_2O vapor makes the lower atmosphere essentially opaque over paths of only a few meters. There is a general trend of decreasing intensities of the lines toward decreasing wavenumbers from the most intense ones near 100 cm^{-1}. Several narrow windows occur below 36 cm^{-1}, and the absorption in each of these windows also generally decreases with decreasing frequency. Transmission measurements have been made in the lower atmosphere for several years in the microwave region below approximately 10 cm^{-1}. Accurate measurements have been difficult to make, but in spite of the difficulties it has been apparent that the window absorption is greater than that predicted by the most widely accepted theoretical line shapes.

In 1968 we[23] made quantitative laboratory measurements of the absorption between 13 cm^{-1} and 36 cm^{-1} by samples of pure H_2O and of H_2O + N_2 at 296 K. As in the infrared windows discussed above, we determined an empirical continuum to include in calculations to bring about agreement with experimental results. It was not possible to determine the influence of changing temperature because all the samples were at the same temperature, 296 K. In 1977, Burch and Clough[24] used laboratory and field data from various workers to derive the curves shown in Figure 10; the data are plotted as attenuation coefficient in dB/km, the units used most frequently for data in this spectral region. These data are based on the MVVW line shape (see Table 1) and apply to an H_2O vapor density of 5.9 gm/m^3. Curve B represents the empirical continuum that must be added to calculated values based on the AFGL line paramaters to bring about agreement with the experimental data represented by the points. Certain simplifications and assumptions were necessarily made so the data could be compared. No allowance was made for temperature. The data points for $\nu \geq 13$ cm^{-1} correspond to laboratory samples at 296 K; most of the other data are from measurements in the lower atmosphere at various temperatures.

---

[23] D. E. Burch, J. Opt. Soc. Am. 58, 1383 (1968)

[24] D. E. Burch and S. A. Clough, Near-Millimeter Wave Technology Base Study in Propagation and Target/Background Characteristics, HDL-SR-79-8 (S. M. Kulpa and E. A. Brown, cochairmen), Harry Diamond Laboratories, Adelphi, Maryland (1979).

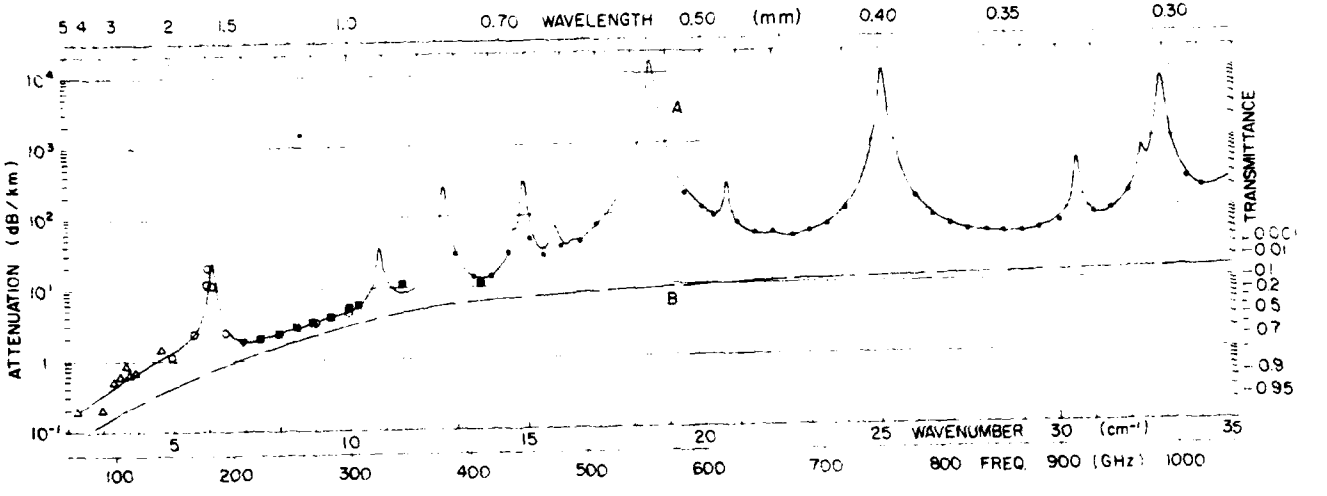

Figure 10. Spectral plots of the near-millimeter attenuation by atmospheric H_2O at sea level. H_2O density = 5.9 gm/m^3. Curve A represents attenuation calculated by summing the theoretical contributions by all the lines and adding the continuum represented by curve B. The data points represent experimental data by: ● Burch[23], ■ Ryadov and Furashov[25], O Frenkel and Woods[25], Δ Straiton and Tolbert[27], and ▼ Dryagin et al[28].

23. D. E. Burch, J. Opt. Soc. Am. 58, 1383 (1968).
25. Ya. V. Ryadov and R. I. Furashov, Radio Phys. and Quantum Electronics 15, 1124 (1974).
26. R. L. Frenkel and D. Woods, Proc. IEEE 54, 498 (1966).
27. A. W. Straiton and C. W. Tolbert, Proc. IRE 48, 898 (1960).
28. Yu. A. Dryagin, A. G. Kislyakov, L. M. Kukin, A. I. Naumov, and L. E. Fedosyev, Isvestya VUZ Radiosphsica 9, 627 (1966).

Burch and Clough recognized the shortcomings of the curves because of the lack of any method to account for temperature changes, and the contribution by self-broadening is not accounted for properly. Users were advised to employ the continuum curve B along with the AFGL fine parameters and assume that the attenuation coefficient was proportional to the H_2O vapor density and to the atmospheric pressure. From Equation (8) we see that this is equivalent to assuming that self-broadening is negligible. Nevertheless, these curves were presented as a basis for calculations until more data could be obtained to determine a more appropriate method of accounting for self-broadening and temperature.

Gaut and Reifenstein[29] have also determined an empirical continuum to account for excess absorption. Their empirical continuum is based on the Gross line shape (see Table 1) and is therefore expected to differ somewhat from the curve of Figure 10, which is based on the MVVW line shape. Gaut and Reifenstein expressed their empirical continuum in terms of the following equation, which has been modified to the notation of the present paper.

$$A_L \quad (\mathrm{dB/km}) = 4.26 \times 10^{-3} \quad (\mathrm{gm/m^3}) \quad \frac{300}{T} \quad 2.1 \; P(\mathrm{atm}) \; \nu^2 \; (\mathrm{cm^{-1}}), \qquad (9)$$

This equation also does not contain a term to account for self broadening, but it does include an empirical factor to account for temperature. This temperature factor may not be accurate for temperatures quite different from 300 K because of inaccuracies in data obtained from many different workers and the relatively narrow range of atmospheric temperatures studied.

The results presented above for the infrared continuum make it clear that the best agreement between calculated and observed window absorption can be obtained by dealing with the N_2 broadening and the self broadening separately. A very strong temperature dependence must also be determined experimentally and taken into account in the calculations. With these observations in mind, we have re-examined many of the published data on microwave and millimeter-wave attenuation, and, to the extent possible, we have analyzed the data by the same methods used in the infrared.

The first step was to analyze the data obtained for pure H_2O samples with emphasis on the window regions where measurements are not sensitive to small errors in wavenumber and where the empirical continuum is most important. In the calculations, we used the Gross line shape because it is the most commonly used in this spectral region. Use of the same line shape makes it easier to compare with other workers' results. As in the infrared windows, the absorption in the millimeter-wave and microwave windows exceeds the absorption calculated from the AFGL line parameters. Values of the excess absorption based on the absorption coefficients reported by several workers are plotted in Figure 11. The solid circles, squares and triangles represent data for which the self-broadening coefficient could be determined directly. The basis for the other points is discussed below. Large variations in the values at the same, or nearby, wavenumbers are obvious. In determining the optimum fit to the scattered data points, it was necessary to make judgments on the validity of each data point. Most weight was placed on results of measurements on samples that produce the most absorption. For example, a result for a sample in a 100-meter multi-pass cell that absorbs 40 percent is given more weight than the result from a 1-meter sample that absorbs less than 1 percent.

---

[29] N. E. Gaut and E. C. Reifenstein III, Environmental Research and Technology Report 13, Lexington, Massachusetts (1971)

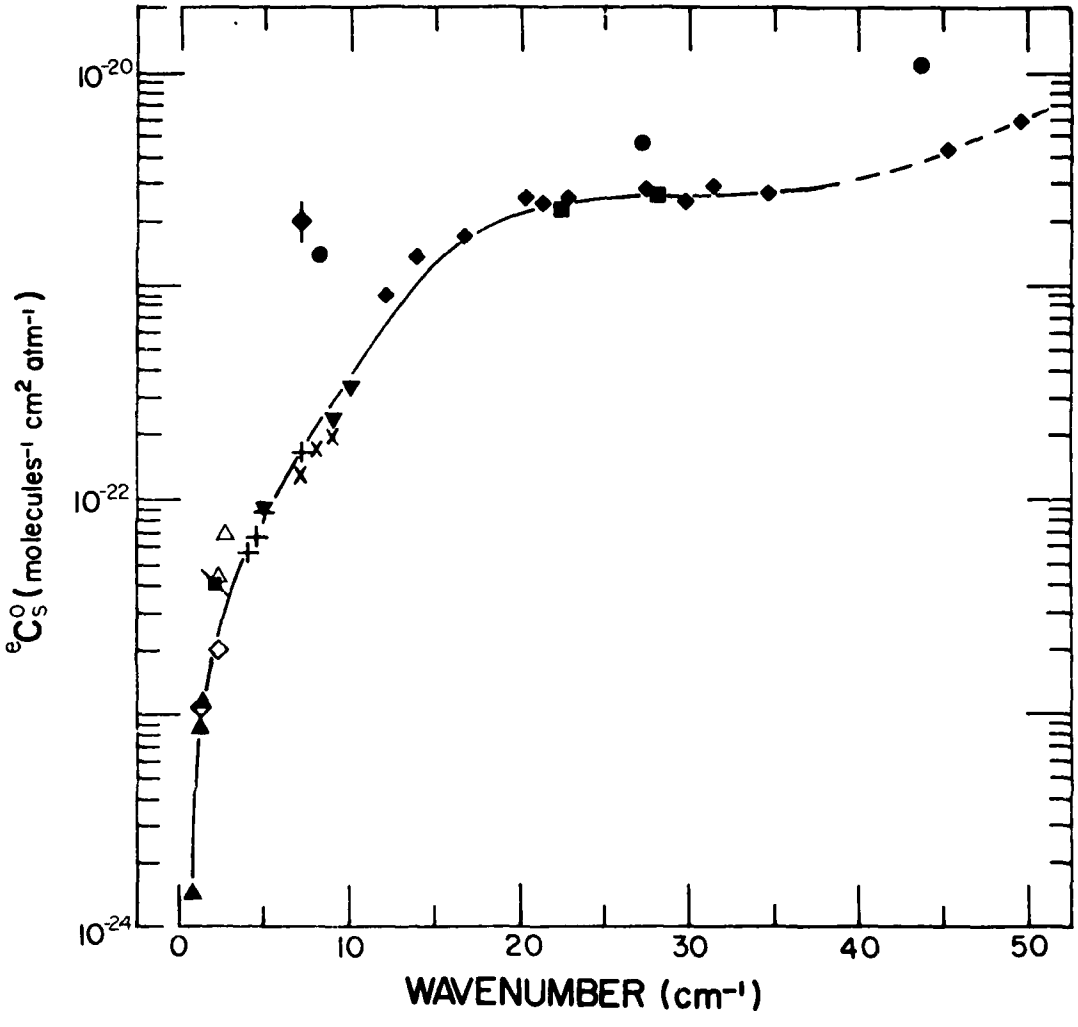

Figure 11. Spectral plot of the empirical continuum for self broadening. ▲ Becker and Autler[30], ■ Liebe[31], ◇ Straiton and Tolbert[27], \ Hogg[32], + Dryagin et al[28], \ Frenkel and Wood[26]; ♦ Llewellyn Jones et al[33], × Ryadov and Furashov[25], ● Simpson et al[34], ◆ Bohlander[35], ■ Burch[23].

30. G. E. Becker and S. H. Autler, Phys. Rev. 70, 300 (1946).
31. H. J. Liebe and T. A. Dillon, J. Chem. Phys. 50, 727 (1969).
32. D. C. Hogg, Measurements of 70- and 80-GHz attenuation by Water Vapor on Terrestrial Path, presented at the URSI-National Radio Science Meeting, Boulder, Colorado (1978).
33. D. T. Llewellyn-Jones, R. J. Knight, and H. A. Gebbie, Nature 274, 876 (1978).
34. O. A. Simpson, S. Perkowitz, R. A. Bohlander, and J. J. Gallagher, Far Infrared Laser Spectroscopy of Water Vapor and Liquid Water, presented at the Fourth International Conference on Infrared and Millimeter Waves and Their Applications, Miami Beach, Florida (1979).
35. R. A. Bohlander,

The short-cell measurement is more subject to error in determining the proper zero-absorption signal and to possible errors due to adsorption of water on the cell windows or to scattered light. The curve in Figure 11 is the best estimate of the proper empirical continuum to represent the excess absorption for pure H_2O samples at approximately 296 K.

As far as is known by this author, only three groups of experimenters have studied samples in such a way as to measure directly the effect of N_2 broadening in this spectral region. The first of these, Becker and Autler,[30] used an untuned cavity to contain samples in which the partial pressure of H_2O was deliberately varied while maintaining a constant total pressure near 1 atm. As expected from Equations (7) and (8), the relationship between attenuation and H_2O partial pressure p contains both a linear and a quadratic term. From the tabulated values of attenuation, we determined both of these terms, which relate directly to C_N^o and C_s^o.

Frenkel and Woods[26] studied samples of pure H_2O and H_2O + N_2 in a tuned cavity and were therefore able to measure quantities related to C_s^o and C_N^o. We were able to determine these constants from data on the samples of H_2O and H_2O + N_2 that we[19] studied in 1968. The curve in the lower panel of Figure 12 is based on these three sets of data, which are represented by the squares and solid triangles.

The curve showing the ratio of the broadening coefficients in the upper panel of Figure 12 is based on the curves of Figures 11 and 12. Note that the minimum value, approximately 14, of this ratio is much larger than 5, the corresponding ratio of the normalized halfwidths for self-broadened and N_2-broadened lines (see Equation (6)). If the empirical continuum were due to the wings of lines and both the self-broadened and N_2-broadened lines had the same shape, the continuum coefficients would each be proportional to α^o and would thus have the ratio of 5:1. The larger observed ratio is consistent with the results obtained in the infrared windows and suggests that self-broadened lines are shaped differently in the extreme wings from N_2-broadened lines.

Values of the ratio $^eC_s^o/^eC_N^o$ from Figure 12 were used in the analysis of the data on air samples represented by the open diamonds, the +'s and the x's in Figures 11 and 12. We assumed that this ratio was valid and calculated both coefficients, $^eC_s^o$ and $^eC_N^o$, from the reported values of attenuation and H_2O partial pressure. Thus, the same measurements are represented in both Figures 11 and 12. The relatively good fit of the open diamonds, +'s and x's to the curve gives strong support for this method of analysis.

Near 10 cm^{-1}, the ratio of coefficients given in Figure 12 is approximately 20:1. In a relatively dry atmosphere containing only 0.5 percent H_2O, the self-broadening contributes only 10 percent of the empirical continuum. However, in a hot, humid atmosphere containing 4 percent H_2O vapor, the self-broadening contributes about 45 percent. Thus, the quadratic term in Equation (7) or (8) is quite significant for high humidities. At low wavenumbers, where the ratio of coefficients may be even greater, the quadratic term may be dominant. In such a case the attenuation in a given path length is nearly proportional to the square of the H_2O partial pressure.

---

[30] G. E. Becker and S. H. Autler, Phys. Rev. 70, 300 (1946)

[26] R. L. Frenkel and D. Woods, Proc. IEEE 54, 498 (1966)

[19] D. E. Burch and D. A. Gryvnak, AFGL-TR-0054, Final Report, Contract F19628-76-C-0302 (1979)

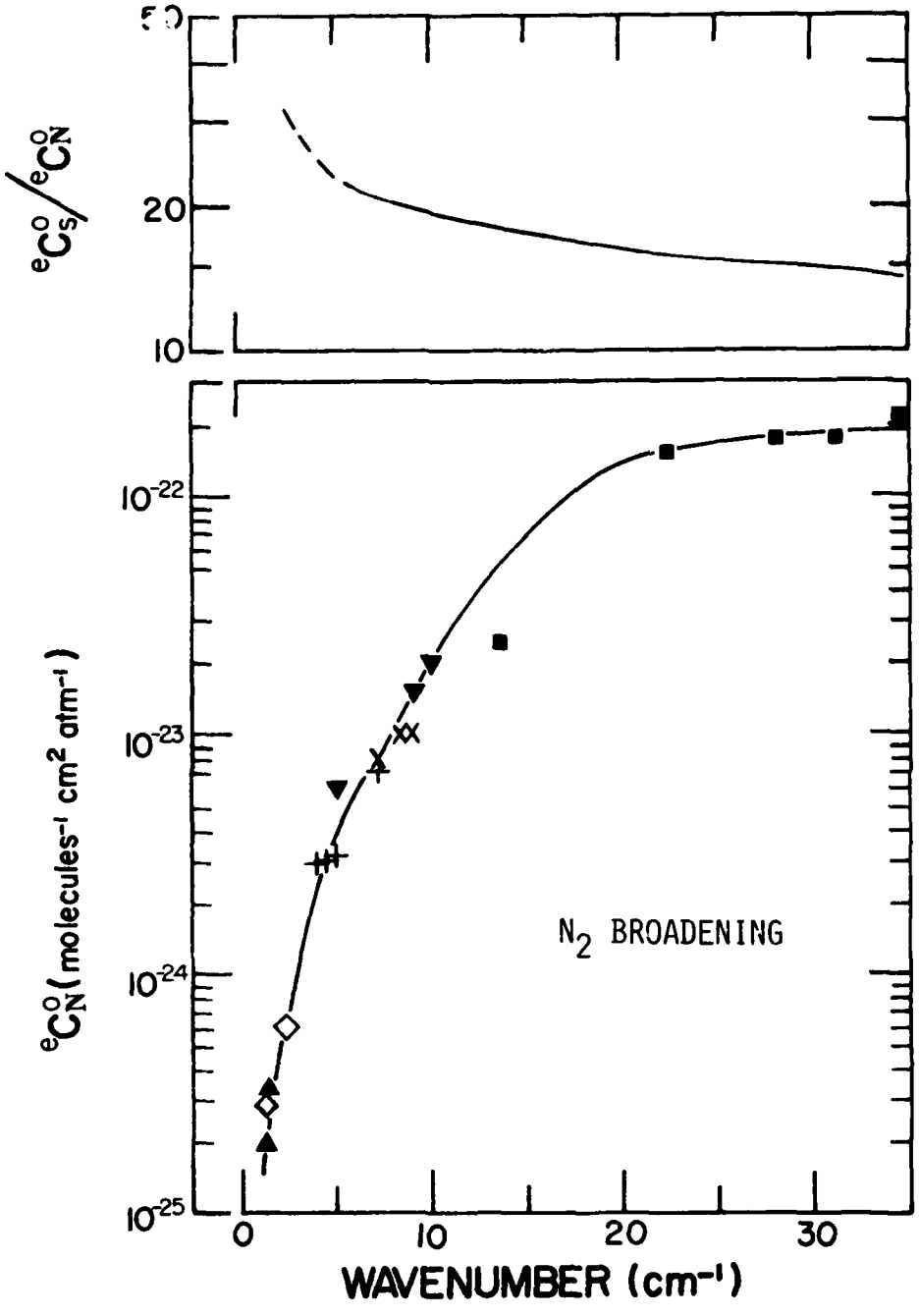

Figure 12. Spectral plot of the empirical continuum for N_2 broadening. The symbols correspond to the same references as those in Figure 11.

Anomalous Absorption

Emery et al[36] have reported horizontal path measurements that indicate anomalous absorption with considerable unexplained structure in the windows between 5 cm^{-1} and 15 cm^{-1}. During their recent work, Rice and Ade[37] encountered some experimental problems involving their Fourier interferometer that can account for false structure such as that reported by Emery et al. Rice and Ade have overcome this problem by improving their calibration technique and have been able to obtain very consistent data in the same spectral region and under atmospheric conditions similar to those studied by Emery et al. All the structure, except that due to O_2 and O_3, observed by Rice and Ade can be explained in terms of the H_2O monomer absorption lines. Ryadov and Furashov[25] measured the attenuation between 5.5 cm^{-1} and 8.5 cm^{-1}, a portion of the region where Emery et al reported anomalous structure, and did not observe any structure except for that due to the H_2O monomer. Thus, until reliable data are obtained and confirmed to indicate otherwise, it is probably best to assume that the H_2O absorption in the near-millimeter wave and microwave regions can be represented by the monomer lines with an empirical continuum that properly accounts for temperature and self-broadening.

COMMON CHARACTERISTICS OF CONTINUUM ABSORPTION

Figure 13 compares the spectral characteristics of the empirical continuum with plots of the absorption coefficient of liquid water and the average intensities of the H_2O vapor absorption lines. The curves were derived in the same way as the curves of Figure 8, which is limited to a narrower spectral interval. In the microwave and millimeter-wave regions, as well as in the infrared, curves C and V have similar relative shapes. The empirical continuum curve, C, is greatest in regions containing very strong absorption lines and is least in the windows. None of the spectral features of curve L, the plot of the coefficient for liquid water, that differ from curve V appear in curve C. This result suggests that the empirical continuum, either in the infrared or at longer wavelengths, is not due to clusters of molecules with liquid-like absorption characteristics. As pointed out in the discussion of Figure 8, these curves suggest strongly that the empirical continuum is related directly to both the vibration and rotation of the normal H_2O monomers. This, of course, would be the case if the empirical continuum is due to the extreme wings of the lines and is required for accurate calculations only because the wrong shape is assumed for the line wings. Clough et al[11] have recently employed a modified VVH (see Table 1) shape to calculate spectra from the microwaves to 5000 cm^{-1}. By employing an empirical correction factor χ they have been quite

---

[36] R. J. Emery, P. Moffat, R. A. Bohlander, and H. A. Gebbie, J. Atmos. Terre. Phys. 37, 587 (1975

[37] D. P. Rice and P. A. R. Ade, Infrared Phys. 19, 575 (1979)

[25] Ya. V. Ryadov and R. I. Furashov, Radio Phys. and Quantum Electronics 15, 1124 (1974)

[11] S. A. Clough, F. X. Kneizys, R. Davies, R. Camache, and R. Tipping, Theoretical Line Shape for H_2O Vapor: Application to Continuum in Atmospheric Water Vapor (A. Deepak, T. D. Wilkerson, and L. H. Ruhnke, eds.), Academic Press, New York (1980)

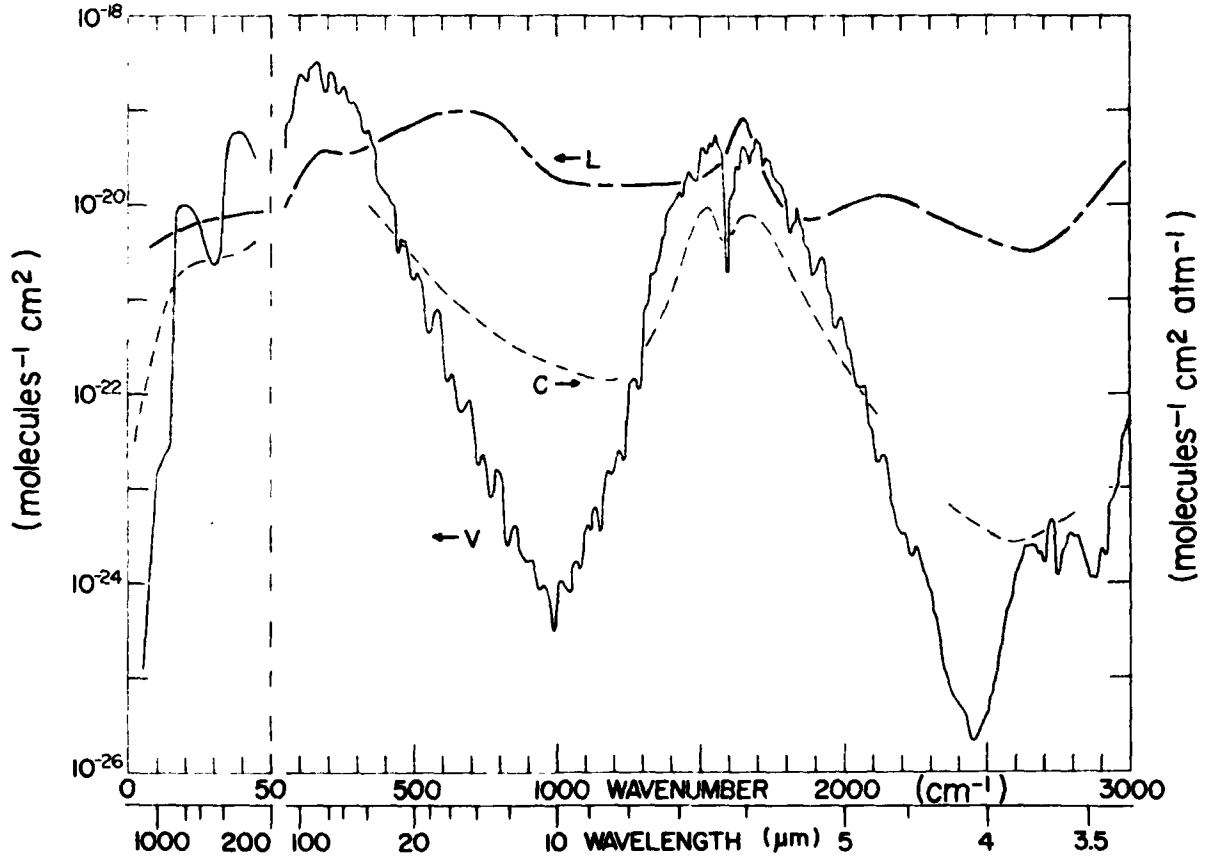

Figure 13. Comparison of the spectral curves from 0 to 3100cm^{-1} of the empirical continuum for self broadening (C), the absorption coefficient of liquid water (L), and the average intensities of the H_2O vapor lines (V). Note scale change at 50 cm^{-1}.

successful in matching experimental results in the well-known windows and in the very narrow windows between the strong lines in the 1200-2300 cm^{-1} region discussed above.

Several workers have suggested that the window absorption increases unusually fast as the humidity level approaches saturation. In order to test this hypothesis while performing some recent, unreported work in the 2400-2600 cm^{-1} region, we deliberately filled the long-path sample cell with pure H_2O until saturation occurred and water condensed on the cell wall. The cell windows and multiple-pass mirrors were heated approximately 3°C above the temperature of the cell wall to avoid condensation on these optical components. As the H_2O partial pressure increased, the transmittance followed, within expected experimental error, the relationship of Equation (7). No unusual changes in transmittance were observed as the sample approached and maintained saturation. Similar experiments should be performed in air samples that contain dust particles or other condensation nuclei that might change the transmittance when the air approaches saturation.

In previous papers[38,39] we have discussed in more detail the changes in C_S^o and C_N^o with changing temperature and distance from the centers of the H_2O lines contributing to the absorption. These papers also point out the similarities in these relationships with those for CO_2, CO, N_2O and other gases.

All of the important characteristics of H_2O absorption in the infrared, millimeter-wave and microwave regions can be explained in terms of collision-broadened lines with shapes that have the following characteristics. For simplicity the shapes are described in terms of the VVH equation with an empirical correction factor χ as discussed in Table 1.

1. When $|\nu - \nu_0|$ is less than about 5 cm^{-1} or 10 cm^{-1}, $\chi = 1$ for infrared lines. This result means that the VVH shape is correct near the center of an infrared line, as are all of the other theoretical shapes represented in Table 1. In the microwave and millimeter-wave regions where ν_0 is small, χ may differ from unity for smaller values of $|\nu - \nu_0|$, but this has not been demonstrated.

2. When $|\nu - \nu_0| \gg \alpha$, χ is a function of $(\nu - \nu_0)$ but independent of α. χ may be asymmetric about $(\nu - \nu_0)$.

3. Self broadening: When $|\nu - \nu_0|$ is greater than about 5 cm^{-1} but less than about 400 cm^{-1} to 500 cm^{-1}, χ is greater than unity. χ is a function of $(\nu - \nu_0)$ and may be as large as 10 or more for some values of $(\nu - \nu_0)$. At low wavenumbers, χ may be a function of ν_0 as well as $(\nu - \nu_0)$.

---

[38] D. E. Burch and D. A. Gryvnak, Continuum Absorption by H_2O Vapor in Atmospheric Water Vapor (A. Deepak, T. D. Wilkerson, and L. H. Ruhnke, etc), Academic Press, New York (1980)

[39] D. E. Burch and D. A. Gryvnak, SPIE Proceedings 142, 16 (1978

4. N_2 broadening: When $|\nu - \nu_0|$ is greater than about 5 cm^{-1} but less than about 100 cm^{-1}, χ is greater than unity; for a given $(\nu - \nu_0)$, χ is less than that for self-broadening. The value of $(\nu - \nu_0)$ beyond which $\chi < 1$ cannot be determined accurately; it is undoubtedly smaller for N_2-broadening than for self-broadening.

5. χ decreases rapidly with increasing temperature. The relative decrease in χ for a given increase in temperature $|\Delta\chi/\chi\ \Delta\theta|$ is much greater for self-broadening than for N_2- broadening. The quantity $|\Delta\chi/\chi\ \Delta\theta|$ also increases with increasing $|\nu - \nu_0|$.

The demonstration that an empirical line shape described by items 1 through 5 can explain most of the characteristics of H_2O absorption does not prove conclusively that it is the correct explanation. The H_2O absorption characteristics could, in principle, be explained by combinations of equilibrium dimers, nonequilibrium dimers, ionic complexes, uncharged complexes, etc., in addition to individual lines. However, it seems improbable that any of these sources other than line wings contribute a major portion of the continuum throughout the entire spectral region. It seems clear that no theoretical line shape derived previously can predict accurately the contributions by line wings. Therefore, there is no justification for the common assumption that any absorption not predicted by line-shape theory is necessarily due to a different mechanism.

SECTION 3

REFERENCES

1. R. A. McClatchey, W. S. Benedict, S. A. Clough, D. E. Burch, R. F. Calfee, K. Fox, L. S. Rothman, and J. S. Garing, AFCRL-TR-73-0096, U. S. Air Force (1973). (Available from NTIS.)
2. D. E. Burch, SPIE Proceedings ___ (1981).
3. K. Bignell, Quart. J. Roy. Meteorol. Soc. 96, 390 (1970).
4. S. S. Penner, J. Quant. Spectrosc. Radiat. Transfer 13, 383 (1973).
5. W. J. Burroughs, R. G. Jones, and H. A. Gebbie, J. Quant. Spectrosc. Radiat. Transfer 9, 809 (1969).
6. M. T. Coffey, Quart. J. Roy. Meteorol. Soc. 103, 685 (1977).
7. D. T. Llewellyn-Jones, R. J. Knight, and H. A. Gebbie, Nature 274, 876 (1978).
8. H. R. Carlon, Infrared Physics 19, 49 (1979).
9. H. R. Carlon, Tech. Report ANCSL-TR-79013, U. S. Army Armament Research and Development Command (1979). (Available from NTIS.)
10. H. R. Carlon, Infrared Physics 19, 549 (1979).
11. S. A. Clough, F. X. Kneizys, R. Davies, R. Camache, and R. Tipping, Theoretical Line Shape for H_2O Vapor: Application to Continuum in Atmospheric Water Vapor (A. Deepak, T. D. Wilkerson, and L. H. Ruhnke, eds.), Academic Press, New York (1980).
12. S. A. Clough, F. X. Kneizys, L. S. Rothman, and W. O. Gallery, SPIE Proceedings 277 (1981).
13. J. H. Van Vleck and D. L. Huber, Rev. Mod. Phys. 49, 939 (1977).
14. D. A. Gryvnak, D. E. Burch, R. L. Alt, and D. K. Zgonc, AFGL-TR-76-0246, Final Report, Contract F19628-76-C-0067 (1976). (Available from NTIS.)
15. D. E. Burch, Semi-Annual Tech. Report, AFCRL Contract No. F19628-69-C-0263, U. S. Air Force (1970). (Available from NTIS.)
16. J. H. McCoy, D. B. Rensch, and R. K. Long, Appl. Opt. 8, 1471 (1969).
17. R. E. Roberts, J. E. A. Selby, and L. M. Biberman, Appl. Opt. 15, 2085 (1976).
18. D. E. Burch, D. A. Gryvnak, and J. D. Pembrook, AFCRL-71-0124, Contract No. F19628-69-0263, U. S. Air Force (1971). (Available from NTIS.)
19. D. E. Burch and D. A. Gryvnak, AFGL-TR-0054, Final Report, Contract F19628-76-C-0302 (1979).
20. B. Farmer, E.M.I. Electronics Ltd., Middlesex, England, Contract No. KH-G-5828-CB19(d)3 (1967).

21. D. E. Burch, D. A. Gryvnak, and G. H. Piper, AFCRA-TR-73-0530, Final Report, Contract F19628-73-C-0011 (1973).
22. G. M. Hale and M. R. Querry, Appl. Opt. 12, 555 (1973).
23. D. E. Burch, J. Opt. Soc. Am. 58, 1383 (1968).
24. D. E. Burch and S. A. Clough, Near-Millimeter Wave Technology Base Study in Propagation and Target/Background Characteristics, HDL-SR-79-8 (S. M. Kulpa and E. A. Brown, cochairmen), Harry Diamond Laboratories, Adelphi, Maryland (1979).
25. Ya. V. Ryadov and R. I. Furashov, Radio Phys. and Quantum Electronics 15, 1124 (1974).
26. R. L. Frenkel and D. Woods, Proc. IEEE 54, 498 (1966).
27. A. W. Straiton and C. W. Tolbert, Proc. IRE 48, 898 (1960).
28. Yu. A. Dryagin, A. G. Kislyakov, L. M. Kukin, A. I. Naumov, and L. E. Fedosyev, Isvestya VUZ Radiosphsica 9, 627 (1966).
29. N. E. Gaut and E. C. Reifenstein III, Environmental Research and Technology Report 13, Lexington, Massachusetts (1971).
30. G. E. Becker and S. H. Autler, Phys. Rev. 70, 300 (1946).
31. H. J. Liebe and T. A. Dillon, J. Chem. Phys. 50, 727 (1969).
32. D. C. Hogg, Measurements of 70- and 80-GHz Attenuation by Water Vapor on Terrestrial Path, presented at the URSI-National Radio Science Meeting, Boulder, Colorado (1978).
33. D. T. Llewellyn-Jones, R. J. Knight, and H. A. Gebbie, Nature 274, 876 (1978).
34. O. A. Simpson, S. Perkowitz, R. A. Bohlander, and J. J. Gallagher, Far Infrared Laser Spectroscopy of Water Vapor and Liquid Water, presented at the Fourth International Conference on Infrared and Millimeter Waves and Their Applications, Miami Beach, Florida (1979).
35. R. A. Bohlander,
36. R. J. Emery, P. Moffat, R. A. Bohlander, and H. A. Gebbie, J. Atmos. Terre. Phys. 37, 587 (1975).
37. D. P. Rice and P. A. R. Ade, Infrared Phys. 19, 575 (1979).
38. D. E. Burch and D. A. Gryvnak, Continuum Absorption by H_2O Vapor in Atmospheric Water Vapor (A. Deepak, T. D. Wilkerson, and L. H. Ruhnke, eds), Academic Press, New York (1980).
39. D. E. Burch and D. A. Gryvnak, SPIE Proceedings 142, 16 (1978)

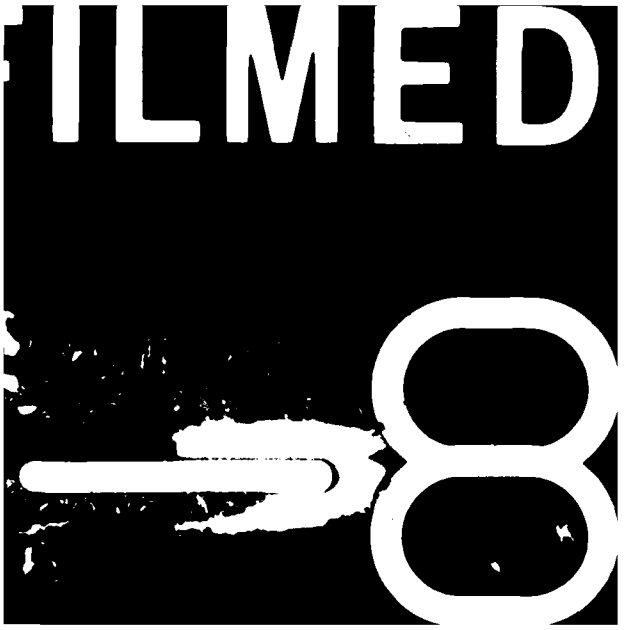
FILMED